MICROSTRUCTURE STUDIES OF POLYCRYSTALLINE

REFRACTORY OXIDES

SUMMARY REPORT

29 March 1972 to 28 April 1973

Contract N00019-72-C-0298

Prepared for

U.S. Naval Air Systems
Washington, D.C.

Approved by

T. Vasilos

T. Vasilos

Prepared by

W.H. Rhodes
P.L. Berneburg
R.M. Cannon
W.C. Steele

AVCO CORPORATION
Systems Division
Lowell, Massachusetts 01851

Approved for Public Release: Distribution Unlimited.

83

AD-760 353

MICROSTRUCTURE STUDIES OF POLYCRYSTALLINE REFRACTORY OXIDES

William H. Rhodes, et al

Avco Corporation

Prepared for:

Naval Air Systems Command

28 April 1973

DOCUMENT CONTROL DATA - R&D

(Security classification of title, body of abstract and indexing annotation must be entered when the overall report is classified)

1. ORIGINATING ACTIVITY (Corporate author)	2a. REPORT SECURITY CLASSIFICATION
Avco Corporation Systems Division Lowell, Massachusetts 01851	Unclassified
	2b. GROUP

3. REPORT TITLE

Microstructure Studies of Refractory Polycrystalline Oxides

4. DESCRIPTIVE NOTES (Type of report and inclusive dates)

Summary Report - 29 March 1972 to 28 April 1973

5. AUTHOR(S) (Last name, first name, initial)

Rhodes, William H.   Steele, Warren C.
Berneburg, Philip L.
Cannon, Rowland M.

6. REPORT DATE	7a. TOTAL NO. OF PAGES	7b. NO. OF REFS
April 1973	95	35

8a. CONTRACT OR GRANT NO.	9a. ORIGINATOR'S REPORT NUMBER(S)
N0019-72-C-0258	
b. PROJECT NO.	
c.	9b. OTHER REPORT NO(S) (Any other numbers that may be assigned this report)
d.	

10. AVAILABILITY/LIMITATION NOTICES

Approved for public release; unlimited distribution

11. SUPPLEMENTARY NOTES	12. SPONSORING MILITARY ACTIVITY
	Naval Air Systems Command Washington, D.C.

13. ABSTRACT

The program was divided into three tasks within the general topic of microstructure effects on the properties of polycrystalline oxides. The press forging process was advanced to the point where a three-inch Al_2O_3 hemisphere of prescribed dimensions could be forged. The product had high transmissivity and a strong crystallographic texture. Initial experiments on press forging Si_3N_4 are reported.

Three grades of powder used in the fabrication of hot pressed 99.9% Al_2O_3 were found to contain particulate impurities which lead to inclusions and/or flaws in the product. Fracture origins were correlated with such flaws or other flawed features of structure in over 70% of the specimens tested. This led to the conclusion that production of high strength Al_2O_3 with a uniform narrow distribution of strength will require improved powder together with careful processing. The findings were discussed in terms of the grain size/ strength curve and the possible pitfall of interpreting fine grains as the initial crack size.

A study of gas/solid interactions in Al_2O_3 showed that CO was the major species evolved from material hot pressed in graphite. The evolution was kinetics limited and not necessary destructive to the structure. The concentration of CO evolved correlated with the powder precursor, but interestingly byproducts of the salt were not detected.

DD FORM 1473

Security Classification

14. KEY WORDS	LINK A		LINK B		LINK C	
	ROLE	WT	ROLE	WT	ROLE	WT
Alumina						
Hot Pressing						
Press Forging						
Mechanical Properties						
Brittle Fracture						
Defect Analysis						
Gases in Ceramics						

INSTRUCTIONS

1. ORIGINATING ACTIVITY: Enter the name and address of the contractor, subcontractor, grantee, Department of Defense activity or other organization (corporate author) issuing the report.

2a. REPORT SECURITY CLASSIFICATION: Enter the overall security classification of the report. Indicate whether "Restricted Data" is included. Marking is to be in accordance with appropriate security regulations.

2b. GROUP: Automatic downgrading is specified in DoD Directive 5200.10 and Armed Forces Industrial Manual. Enter the group number. Also, when applicable, show that optional markings have been used for Group 3 and Group 4 as authorized.

3. REPORT TITLE: Enter the complete report title in all capital letters. Titles in all cases should be unclassified. If a meaningful title cannot be selected without classification, show title classification in all capitals in parenthesis immediately following the title.

4. DESCRIPTIVE NOTES: If appropriate, enter the type of report, e.g., interim, progress, summary, annual, or final. Give the inclusive dates when a specific reporting period is covered.

5. AUTHOR(S): Enter the name(s) of author(s) as shown on or in the report. Enter last name, first name, middle initial. If military, show rank and branch of service. The name of the principal author is an absolute minimum requirement.

6. REPORT DATE: Enter the date of the report as day, month, year; or month, year. If more than one date appears on the report, use date of publication.

7a. TOTAL NUMBER OF PAGES: The total page count should follow normal pagination procedures, i.e., enter the number of pages containing information.

7b. NUMBER OF REFERENCES: Enter the total number of references cited in the report.

8a. CONTRACT OR GRANT NUMBER: If appropriate, enter the applicable number of the contract or grant under which the report was written.

8b, 8c, & 8d. PROJECT NUMBER: Enter the appropriate military department identification, such as project number, subproject number, system numbers, task number, etc.

9a. ORIGINATOR'S REPORT NUMBER(S): Enter the official report number by which the document will be identified and controlled by the originating activity. This number must be unique to this report.

9b. OTHER REPORT NUMBER(S): If the report has been assigned any other report numbers (either by the originator or by the sponsor), also enter this number(s).

10. AVAILABILITY/LIMITATION NOTICES: Enter any limitations on further dissemination of the report, other than those imposed by security classification, using standard statements such as:

(1) "Qualified requesters may obtain copies of this report from DDC."

(2) "Foreign announcement and dissemination of this report by DDC is not authorized."

(3) "U. S. Government agencies may obtain copies of this report directly from DDC. Other qualified DDC users shall request through

_____."

(4) "U. S. military agencies may obtain copies of this report directly from DDC. Other qualified users shall request through

_____."

(5) "All distribution of this report is controlled. Qualified DDC users shall request through

_____."

If the report has been furnished to the Office of Technical Services, Department of Commerce, for sale to the public, indicate this fact and enter the price, if known.

11. SUPPLEMENTARY NOTES: Use for additional explanatory notes.

12. SPONSORING MILITARY ACTIVITY: Enter the name of the departmental project office or laboratory sponsoring (paying for) the research and development. Include address.

13. ABSTRACT: Enter an abstract giving a brief and factual summary of the document indicative of the report, even though it may also appear elsewhere in the body of the technical report. If additional space is required, a continuation sheet shall be attached.

It is highly desirable that the abstract of classified reports be unclassified. Each paragraph of the abstract shall end with an indication of the military security classification of the information in the paragraph, represented as (TS), (S), (C), or (U)

There is no limitation on the length of the abstract. However, the suggested length is from 150 to 225 words.

14. KEY WORDS: Key words are technically meaningful terms or short phrases that characterize a report and may be used as index entries for cataloging the report. Key words must be selected so that no security classification is required. Identifiers, such as equipment model designation, trade name, military project code name, geographic location, may be used as key words but will be followed by an indication of technical context. The assignment of links, rules, and weights is optional.

MICROSTRUCTURE STUDIES OF POLYCRYSTALLINE

REFRACTORY OXIDES

SUMMARY REPORT

29 March 1972 to 28 April 1973

Contract N00019-72-C-0298

Prepared for

U.S. Naval Air Systems
Washington, D.C.

Approved by

T. Vasilos

Prepared by

W.H. Rhodes
P.L. Berneburg
R.M. Cannon
W.C. Steele

AVCO CORPORATION
Systems Division
Lowell, Massachusetts 01851

Approved for Public Release: Distribution Unlimited.

FOREWORD

This report was prepared by the Systems Division of Avco Corporation under U.S. Navy Contract N00019-72-C-0298 entitled, Microstructure Studies of Polycrystalline Oxides.

The work was administered under the direction of the U.S. Department of the Navy, Air Systems Command, with Mr. Charles F. Bersch, Code AIR-52032A, acting as Project Engineer.

This report covers work conducted from 29 March 1972 to 28 April 1973.

The writers are pleased to acknowledge the contributions of the following individuals to this program; B. MacAllister for mechanical evaluation, C.L. Houck for ceramographic preparation, J. Centorino, P. Foley, G. Ross, and E. Vallante for materials preparation, and T. Vasilos for useful discussions. Also Dr. N. Dutta of the U.S. Army Materials and Mechanics Research Center is acknowledged for helpful discussions in the area of flaw analysis.

TABLE OF CONTENTS

LIST OF ILLUSTRATIONS

LIST OF ILLUSTRATIONS (Concl'd)

LIST OF TABLES

I. INTRODUCTION

Three aspects of oxide fabrication and properties were studied. They were treated as separate topics although there were implications and inter-relations from one topic to the next. Each topic was at a different stage in development and knowledge. The press forging of Al_2O_3 has been under study for a number of years; thus, the current effort dealt with developing the processing to allow fabrication of useful shapes. A few preliminary experiments on the application of the press forging process on Si_3N_4 are reported. One year of effort has been given to finding the cause of the low strength Al_2O_3 bars in a distribution of bars with various strengths. This study was continued with characterization of two new sources of powder and the resultant product. A new area was undertaken for study this year that has an obvious interrelationship with the others. Gaseous species in hot pressed products are well known, but their origin, level of concentration, and effect on properties have received only limited study. This initial effort dealt with the identification of the gas phase, possible chemical reactions, and the relationship between precursor of the Al_2O_3 powder and gases evolved from the hot pressed product.

II. PRESS FORGING OF ALUMINA HEMISPHERES

A. General

Press forging polycrystalline Al_2O_3 has previously established[1] that high density bodies can be achieved with unique properties. High in-line optical transmissivity is obtained as a result of nearly complete pore removal and high crystallographic texturing. The textured structure is achieved by plastic deformation primarily on the basal slip system. This texture is retained through primary recrystallization.

Porosity distributed throughout the structure may act as preferred nucleation sites for the new generation of grains during recrystallization. This process itself could absorb porosity or the structure could be more susceptible to continued densification due to the nearness of pores to grain boundaries; their potential sink. In-line light transmissions of 60% at 0.7 μ wavelength were achieved for the forged material as compared with a maximum of 20% for the best randomly oriented pore-free Al_2O_3 available at an equivalent thickness. This resulted from the preferred basal texture eliminating to a large extent the light diffraction due to birefringence. Inverse pole figures demonstrated that the crystallographic orientation was strong but not perfect. The misorientation undoubtedly accounts for the absence of even higher optical transmission figures.

Mechanical strength was the second property that was enhanced as a result of forging. It was found that the strength at -196°C and 1200°C was nearly independent of grain size in the 1-20 micron range[1c,d]. Fracture strengths in the 1200° to 1450°C range were over 50% higher than straight hot pressed material of an equivalent grain size[1e]. However, there was no apparent effect of texture on the plastic properties between 1475°-1700°C[1d].

Most recently thin shell 2-inch diameter hemispheres have been forged which retain the crystallographic orientation in the plane of the

shell.[1h] The optical transparency was uniform throughout the full hemisphere on the best samples. During forging of the sintered preforms, edge tears developed in the skirt of the forging, and some of these extended from the 0.4-inch skirt into the hemisphere portion of the forging. The tearing was thought to ' cavitation resulting from a more rapid deformation than the available mechanisms could accommodate at the strain rate imposed. This problem was one of the subjects addressed in the current effort. The second major effort was aimed at developing the process to the point where a specific geometry could be achieved. Along with this effort, the process was scaled up to a three-inch diameter hemisphere.

B. Raw Materials and Preforms

Vendors I and II 99.98% Al_2O_3 powder was used for the forging experiments. Section II includes a description of these powders. Concentrations between 0.12 and 0.03% weight percent MgO were added to an alcohol/alumina slip in a ball milling operation. The dried powder was isostatically pressed at 20 Kpsi into cylinders 3 inches diameter by 4 inches long. These were cut and shaped in the green state into circular right cylinders 2-inch diameter by 1½-inch high with a 2-inch radius cap. Some of the preforms were used in the green state while others were fired in H_2 at 1500°C which resulted in relative density of about 98.5%. It was of interest to forge some of the higher density preforms as they were expected to have closed pores, and H_2 is more soluble in Al_2O_3 than other gases.[2]

C. Press Forging Procedure

Forging runs were conducted in an induction heated 75 ton press using standard ambient graphite base hot pressing furnace construction techniques. The forging die was constructed from high strength HPD Poco graphite. The material nearly matches the thermal expansion coefficient of Al_2O_3. This turns c to be a big advantage in die design as dimensions can be directly translated. Also, problems of specimen/die thermally induced cool down constraints are greatly minimized using Poco graphite. The die was designed to produce a 1.52-inch radius hemispherical cap end with a 0.4-inch high 8° tapered cylindrical skirt. A pinned top ATJ punch was used which allowed hot extraction of the male die. The boron nitride die lubricant was sprayed or painted directly onto graphite. In some cases, graphite paint was used between the male punch and BN cover coat. Ambient atmosphere forgings were employed which meant that at the forging temperature the atmosphere was predominantly CO with a partial pressure of CO_2 and A. The argon permeated into the cavity from the sight tube where it was employed as a sight tube flush. Also, residual nitrogen was expected.

The die assembly was heated to the forging temperature in about 100 minutes. The ram travel was initiated and driven by a manual strain rate control. The strain rate during the rapid deflection regime was controlled to between 1×10^{-4} sec^{-1} and 1×10^{-3} sec^{-1}. The above strain rates are the best present estimates of acceptable strain rates in the 1850°C range. Once maximum pressure was reached, the deflection rate slowed down as forging and densification came to a conclusion. The specimen was held at maximum temperature and pressure for some prescribed period of time beyond that where deflection has apparently ceased. Some densification

continues by diffusion, and there is some evidence that multiple recrystallization may take place in this period[1b]. Upon completion of the run, pressure was released and the male punch extracted.

D. Analysis

The texture or degree of crystallographic orientation in forged materials is best determined by X-ray diffraction techniques. Such information, of course, is of great benefit in the interpretation of the forging studies. Texture is completely described by the construction of a pole figure which shows the distribution of the orientations of the various crystallographic axes of the individual crysta lites in the polycrystalline body relative to the axes of the forging process. However, for the purpose of evaluating relative degrees of orientation, a simpler system was devised.

The diffraction pattern of a random (powder) sample was obtained. Values of $f_o (I_{hkl})$ or normalized intensities defined by the relation

$$f_o(I_{hkl}) = \frac{I(hkl)}{\sum_{h,k,l} I(hkl)}$$

were calculated for each of a number of reflections from planes at various angular orientations with respect to the basal plane.

Similarly, values $f(I_{hkl})$ were calculated from the diffraction pattern of a flat ground surface on a forged specimen. The ratios of the normalized intensities for the respective reflections $R(I_{hkl}) = \dfrac{f(I_{hkl})}{f_o(I_{hkl})}$

which give the relative intensity of reflection are calculated and plotted against the angle ϕ between the planes (hkl) and the basal plane.

In the case of a random powder sample, R has the constant value of unity over the entire ϕ range. In the case of a perfectly oriented sample, R is zero everywhere except at $\phi = 0$ where it has some large finite value. In the case of a distribution of orientation, in general, R will decrease monotonically from $\phi = 0$ to $\phi = 90°$. The better the crystallites are aligned, the higher the intercept at $\phi = 0$ and the steeper the drop with increasing ϕ.

Specimens 1/8-inch square were extracted from forged billets. The center of these specimens was 13/16 inch from the center of the billet so a comparison of orientation data between billets gave an accurate view of relative orientation without fully describing relative orientation along a radius in any given billet.

E. Forging Results and Discussion

The experiments are listed chronologically in Table I. After an initial commissioning run (1826), a series of five runs employing sintered preforms were conducted. Several of these runs were quite successful and new insight was gained in this initial series. It was determined after

TABLE I

Hemispherical Alumina Forging Experiments

Experiment	Powder	Preform Prep.	Preform Density	Separating Media*	Temp. °C (corrected by 65°C)	Pressure psi	Time** min.	Density gm/cc	Remarks
1826	M-1 0.12 MgO	Cold Press	2.0	BN/BN Dylon	1905	6250	100 (185)	3.63	90° of arc forged, badly cracked edges.
1830	L-1 0.05 MgO	Cold Press Sinter H_2	3.92	BN/BN Dylon	1890	6250	210 (265)	3.92	Full hemisphere translucent, stuck on male punch, apex cracked, minor rim cracks.
1832	L-1 0.05 MgO	Cold Press Sinter H_2	3.93	BN/BN Dylon	1885	6250	75 (180)	3.89	Full hemisphere translucent, rim cracks extend 0.25" into hemisphere, hot extracted into female. 4
1834	L-1 0.05 MgO	Cold Press Sinter H_2	3.93	BN/BN Dylon	1885		220 (330)	3.91	Full hemisphere forged with almost no rim cracks; badly reacted, cracked, stuck on male.
1838		Cold Press Sinter H_2		BN/BN Dylon	1880	6250	35 (180)	3.85	120° of arc translucent, uneven wall thickness; rim cracks extend 0.45" into hemisphere.
1840	L-1 0.035 MgO	Cold Press Sinter H_2		BN/BN Dylon	1895	5700	13 (165)	3.95	Full hemisphere translucent, one rim crack extending 0.45" into hemisphere, one crack extends to apex, slight reaction on I.D, stuck on male.

Experiment	Powder	Preform Prep.	Preform Density	Separating Medium	Temp. °C (corrected by 65°C)	Pressure psi	Time** min.	Density gm/cc	Remarks
1857	L-1 0.035 MgO	Cold Press Sinter H_2		BN/BN	1885	5700	20 (128)	3.96	60° of arc translucent; rim cracks extend 0.5", uneven wall thickness.
1866	L-1 0.035 MgO	Cold Press		BN/BN	1565 1885	5950 6250	60 (85) 50 (67)	3.77	Not fully forged (insufficient powder). Edge cracks extend 0.75", opaque, no apex cracks.
1874	M-1 0.035 MgO	Cold Press	1.81	BN/BN	1585 1885	4500 6250	30 (50) 77 (85)	3.93	90° arc translucent, one chip out of apex, no cracks, uneven wall thickness.
1874 re-run					1885	0	180	3.80	Opaque.
1875	M-2 0.035 MgO	Granulated Powder	1.81	BN/BN	1585 1885	6250 6250	35 60	3.69	Opaque, uniform wall thickness, no cracks, initial pressure applied at 1000°C.
1878	M-1 0.035 MgO	Cold Press	1.80	BN/BN	1565 1885	4500 6250	60 60	3.76	Opaque, healed apex cracks.
1879	M-1 0.035 MgO	Cold Press Sintered H_2		BN/BN	1615	6500	30		Punch broke - not fully forged.
1889	M-1 0.035 MgO	Cold Press	1.80	BN/BN	1880	6250	60	3.96	180° of arc translucent, healed apex cracks, initial pressure applied at 1615°C.
1891	M-1 0.035 MgO	Cold Press	1.80	BN/BN	1665 1885	2840 6250	30 30	3.91	Opaque rim and apex cracks.

Experiment	Powder	Preform Prep.	Preform Density	Separating Media*	Temp.°C (corrected by 65°C)	Pressure psi	Time** min.	Density gm/cc	Remarks
1893	M-1 0.035 MgO	Cold Press	1.80	BN/BN	1875	6250	40	3.96	Opaque, no cracks, initial pressure applied at 1585°C.
1895	M-1 0.035 MgO	Cold Press	1.80	BN/BN	1875	6250	30	3.97	Opaque, rim and apex cracks, initial pressure applied at 1985°C.
1898	U-1 0.035 MgO	Cold Press	1.80	BN/BN	1875	6250	50	3.95	Opaque apex cracks, initial pressure at 1520°C.
1899	U-1 0.035 MgO	Cold Press	1.80	BN/BN	1885	6250	60	3.95	Opaque, apex cracks, slight reaction problems, initial pressure at 1520°C.

*Coating for female listed first.

**First time is time at temperature and pressure, and time in parenthesis is time at temperature. The difference is the time of load application.

examining runs Nos. 1834 and 1840 that a pressing temperature of $1885^{\circ}C$ to $1895^{\circ}C$ was on the ragged edge of a temperature where a reaction between Al_2O_3 and the die or separator materials proceeded at a measurable rate. This reaction rate was sufficient to cause serious problems with a 330-minute hold, lesser problems with a 165-minute hold, and almost no problems with a 128-minute hold. A drop of about $10^{\circ}C$ apparently eliminated the problem even for long holds at temperature. The reactions did cause some of the cracks that extended into the apex. Two other runs provide some insight into the problem of cracking. It was originally thought that the apex crack of No. 1830 was caused by thermal expansion mismatch as it was stuck slightly to the male punch. However, Run 1838 was also stuck to the male punch and did not exhibit any apex crack. This finding was borne out by subsequent runs. Thermal shock was ruled out after numerous runs survived the furnace cooling without cracking. In fact the apex crack of No. 1830 was not convincingly explained, and may be related to stress components of the rim cracks.

Rim cracking was a problem that was carried over from the previous effort. It was common to develop 5 to 6 rim cracks as shown in Figure 1. These rim cracks, in general, extended for the full 0.4 inch of the disposable skirt. The rim cracks were thought to arise due to cavitation resulting from the imposition of strain rates greater than the available deformation mechanisms could tolerate. It is known that basal slip plays a major role in the deformation, but accommodation must be accounted for by diffusional creep with a grain boundary sliding component. One of these mechanisms must control the steady state flow stress at $1880^{\circ}C$, and therefore the onset of cavitation if the strain rate is exceeded. If work in the $1300-1600^{\circ}C$ range can be extrapolated to the higher temperature, it would appear that diffusional creep may be the controlling deformation process.[3] An effort was made to control the imposed strain rate through load rate control. Figure 2 illustrates the deflection and range of strain rates for several runs during the series (1830 to 1857) using sintered preforms. Run 1832 exhibited a peak in the strain rate curve at 35 minutes. Strain rate control had improved by the time Run 1840 was made as the curve slowly decreased during the run as it probably should to allow for the decreasing flow stress associated with grain growth. This level of strain rate was still apparently too fast as rim cracks were present. Run 1834 exhibited only 3 rim cracks 0.2-inch long, but, of course, this sample was spoiled because of the reaction problem. However, the results suggest that the temperature was just enough higher to provide the margin needed to prevent serious rim cracking. This, together with the reaction, suggest that the temperature may have been higher than the $1885^{\circ}C$ recorded. Thus, it is thought that further refinements in the direction of even lower strain rates may provide the margin needed to control the rim cracks to a tolerable level.

As mentioned, the rim cracks are concentrated in the disposable skirt. Consequently, several of the hemispheres produced in this initial series were crack-free within the hemisphere desired as a final product. Figure 3 illustrates a machined and polished hemisphere taken from forging 1857. The "as-forged" version was illustrated in Figure 1. The product was quite transparent and appears to hold considerable promise for optical applications.

Run 1866 was conducted under conditions which represented a marked

5751-5 1X

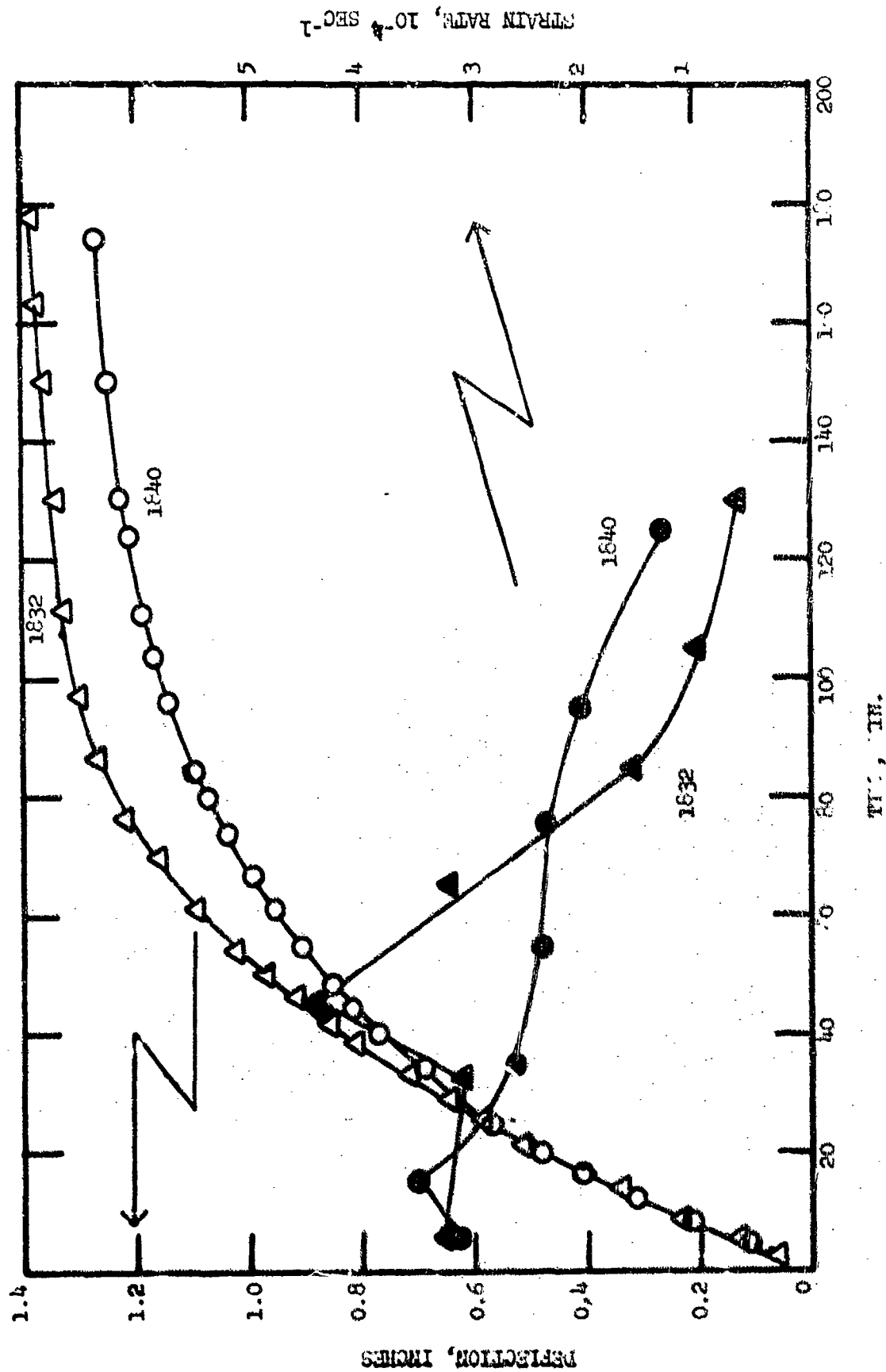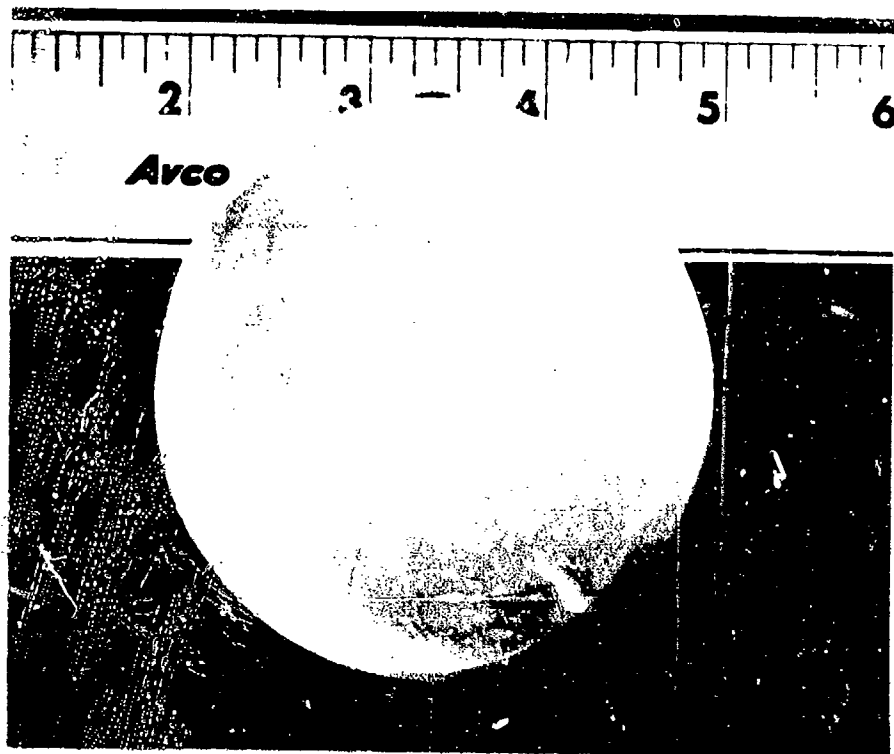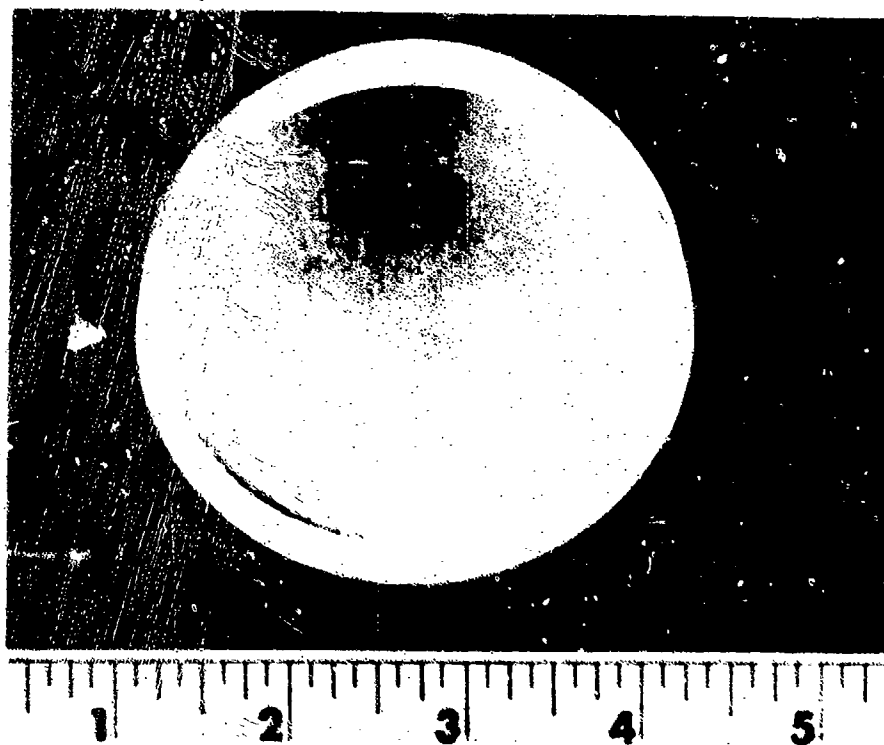Figure 1. Forging 1857 Showing Rim Cracks in Skirt of As-Forged Hemisphere.

Figure 2. Deflection and Strain Rate Curves for Hemispherical Forms, 1832 and 1840.

Figure 3. Polished Hemisphere from Forging 1857.

departure from the initial series. A cold pressed preform was employed
in place of a sintered preform, and forging commenced at 1565° rather than
1880°C. The use of a cold pressed preform was expected to yield benefits
in increased ductility due to the finer grain size and increased accommoda-
tion of a high porosity body. Flat forgings of such material have been
previously reported[14e]. The piece was forged in two stages as inferred
from Table I. The piece showed definite promise for the approach, but there
were several features requiring improvement. Rim cracks were present even
though far fewer formed and those were partially healed. Unfortunately,
the preform did not weigh enough resulting in a piece not fully forged and
not fully dense. The approach appeared worthy of continued emphasis.
Run 1874 also employed an isostatic cold pressed billet and again a two-step
approach was taken. In the initial phase at 1585°C, the strain rate was
reduced and only 4500 psi was applied in an effort to avoid rim cracks.
After a 30-minute hold at this temperature, power was increased raising the
temperature to 1885°C. At this point the pressure was raised to 6250 psi
with a velocity goal of ≤ 0.015 inch/min. The forging was very successful
as it was crack-free throughout, and exhibited high translucency for about
90° of arc. One chip flaked out near the apex leaving the wall thickness
about 0.100 at this point. The cause of this chipping was a very slight
sticking and reaction similar to what happened on a more extensive basis
for runs 1834 and 1840. The wall thickness was not uniform indicating
that this can be a problem for both cold pressed and sintered preforms.

The use of cold pressed preforms was followed for much of the
remaining work since it offered a ready solution to the rim cracking problem.
Runs 1874, 1875, and 1893 were successfully forged and had no rim cracks.
Figure 4 illustrates the type of product obtained in this series. These
specimens were not highly translucent, but this was due to deliberately
restricting the hold time at maximum temperature. During this phase of the
experiment, the principal goal was the elimination of rim cracks. Samples
1878 and 1889 exhibited healed cracks which were judged to be a result of
fracturing the preform early in the run. The cold pressed preform has a
much lower strength than the sintered preforms. Thus, it is reasonable to
expect that lower stresses and strain rates can be tolerated until densifica-
tion approaches 99% of theoretical. Analysis of the run conditions for
these cracked forgings compared with the uncracked forgings pointed to
high stress at an early stage in the process being more critical than high
strain rates.

One possible solution to the reaction problem would be to simply
forge using a minimal thermal cycle to achieve the orientation and a
moderately high density. This could be followed by a sintering anneal to
attain a high degree of transparency. Run 1874, which had been forged
from a powder preform, was sintered in an ambient hot pressing environment
for 3 hours at 1865°C. Instead of sintering, a 3% loss of density was
recorded. This was a clear example of the problem of gases in hot pressed
(and apparently forged) ceramics which is discussed more fully in Section
IV. It is thought that sintered preforms subsequently forged and re-
sintered would not display this behavior due to H_2 being the residual gas
phase and the fact that H_2 is apparently soluble in Al_2O_3.[2,33]

5751-7   1X

Figure 4. Forging 1893 from a powder preform illustrating elimination
           of rim cracks.

Run 1875 was in reality a hot pressing rather than a forging. Granulated (-100 mesh) powder was loaded into the die nearly filling the female cavity. The initial pressure was applied at $1000^{\circ}C$ which is fairly common practice in hot pressing. The sample was uncracked, and probably unoriented. It was 92.5% dense which, of course, is not impressive, and suggests that this is not a very desirable approach.

Forging 1879 was performed on a sintered preform at $1615^{\circ}C$ which was $200^{\circ}C$ lower than any previous hemispherical forging. Previous efforts had taught that forgings could be conducted as low as $1400^{\circ}C$ and, furthermore, crystallographic orientation was achieved.[3] However, forging 1879 was unsuccessful as the forging die fractured at a stress which was at least 6500 psi and possibly as high as 20,000 psi (uncertainty due to possible error in area of preform in contact with die). No further efforts were made at low temperature forgings. The concept appears worthy of further consideration although it is clear that a delicate balance exists between deformation stresses and strength of the die components. As with all the forgings, a balance between grain growth and flow stress must also be found.

Forgings 1891, 1898, and 1899 were performed using a die set fabricated from ATJ graphite. It is noteworthy that all of these forgings stuck on the male punch and were badly cracked. This was attributed to the mismatch in thermal expansion between this grade of graphite and Al_2O_3.

F.   Characterization Results and Discussion

Forging 1830 was sectioned and examined at mid section and near the inner rim (Figure 5). Second phase similar to that previously encountered was apparent at mid section (arrow D). The area where a slight reaction was visible showed a third phase (arrow A). The phase at arrow B appeared similar in reflectivity to the arrow D phase, but, of course, in much higher concentration. X-ray analysis was performed by a diffractometer trace on the outer hemispherical surface. The major phase was $\propto$-Al_2O_3. Also found were a spinel-type ($a_o \sim 7.94$) and a third phase which could possibly be AlN, BN, H_3BO_3, or a tetragonal Al-O-N compound. Previously[14], the spinel-type second phase was identified as $MgAl_2O_4$. Pressing 1830 contained only 0.05% MgO which was about 100 ppm under the solid solution limit at $1830^{\circ}C$ in vacuum. In reconsidering the problem, it was thought that the second phase might be an oxynitride of the type Al_2O_3 . AlN. One form of this phase is reported to be a spinel face centered cubic structure with compositionally dependent lattice parameters which include the value 7.95 Å.[4] Electron microprobe analysis was performed on this sample in an effort to clarify principally the question of matrix second phase identification. Nitrogen was found in the phase identified by arrow A of Figure 5, but not in any other phase. The phases delineated by arrows B and D were rich in Mg while no Mg was found in the phase under arrow C. Only Al emission was noted here. Based on these analyses, the phase identification can be narrowed down to either AlN or BN for the phase at arrow A and $MgAl_2O_4$ solid solution for the phases at arrows B and D. It may be possible for N to enter into the $MgAl_2O_4$ structure based on the similarity in structure for the oxynitride.
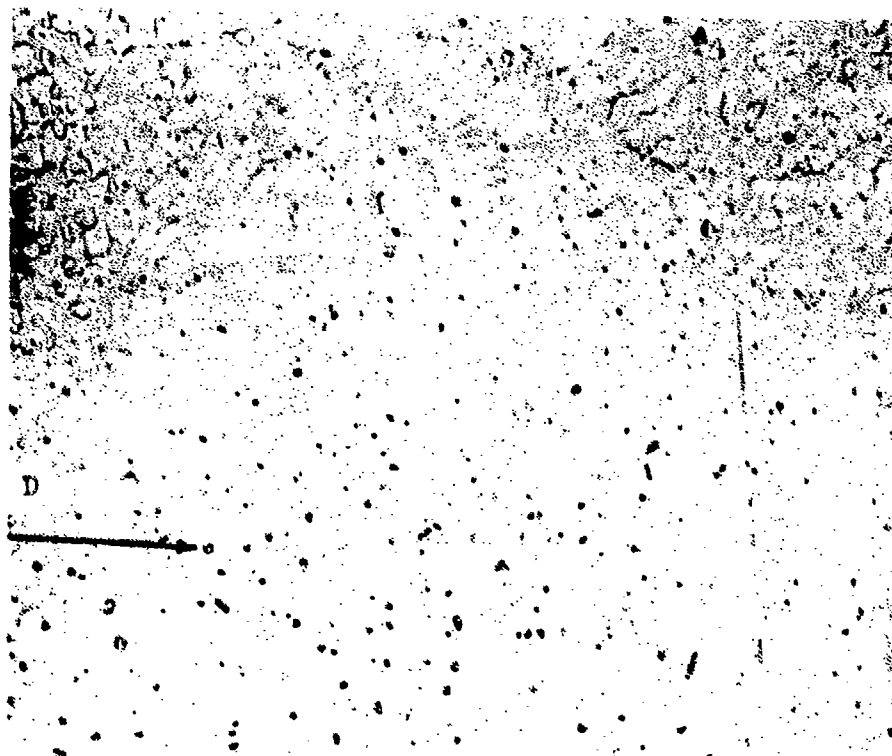
Based on the fact that BN was in contact with the sample surface during forging, the phase at arrow A is probably BN. The high concentration
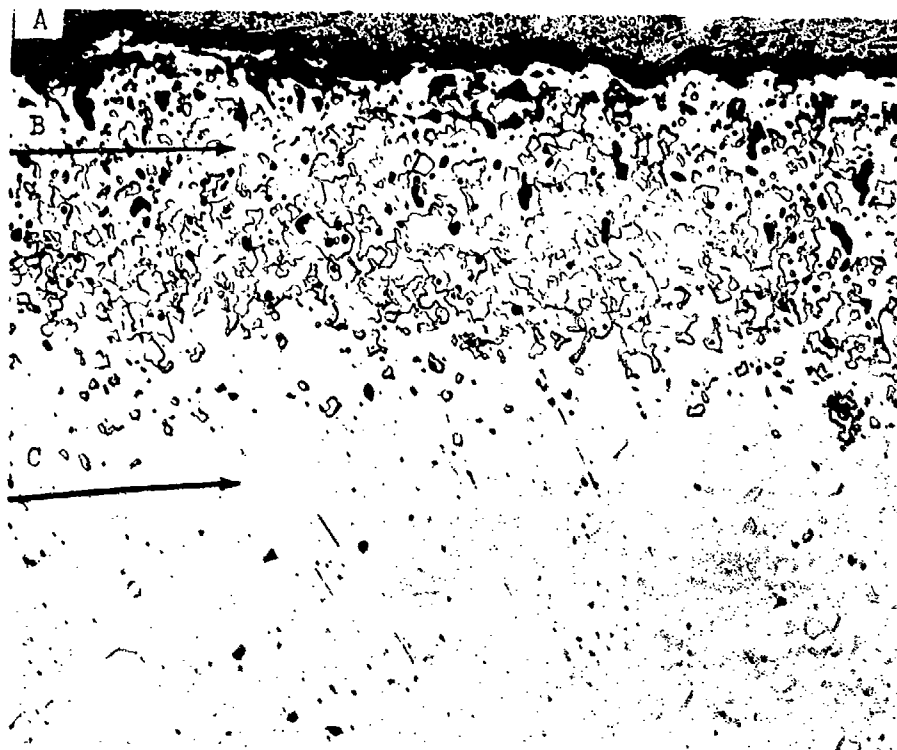
5697-1   (a)   100X

5697-2   (b)   100X

Figure 5. Section of (a) rim and (b) center of 1830 Al_2O_3 Hemisphere Forging.

of $MgAl_2O_4$ at the surface must arise from normal volatilization of MgO at high temperatures. Being confined by the forging die, this phase must react to form $MgAl_2O_4$. This phase in turn appears to bond preferentially (over Al_2O_3) with BN. No clearcut reaction phase was found, but it is suggested that some of the sticking problems and reaction problems were caused by a reaction of BN and $MgAl_2O_4$.

Figure 6 illustrates the microstructure of a 0.035 wt. % MgO addition to Al_2O_3 after forging at 1885°C. The $MgAl_2O_4$ concentration was found to be 0.45 vol. % by lineal analysis with no geometric correction. This analysis together with others performed on various 1880° - 1890°C forgings having additions of MgO to Al_2O_3 are plotted in Figure 7. Judging by the extrapolation of this data, the solubility limits of MgO is estimated to be about 0.015 wt. %. This, of course, should be added to the background concentration which according to the lot analysis of the powder employed for the lowest two MgO additions was a "trace". This is assumed to be $\leq$ 50 ppm making the observed solubility limit $\sim$0.02 wt. % at $\sim$ 1880°C in an atmosphere which must be >99.9% CO.

Roy and Coble[5] measured the MgO solubility in Al_2O_3 in vacuum. At 1880°C, which is only a 50°C extrapolation of their data, they expect a 0.0880 wt. % MgO solubility. Samples equilibrated in H_2 showed a slight shift in lattice parameter, whereas those prepared in vacuum or air did not exhibit a shift in lattice parameter. This was interpreted as evidence for even greater solubility of MgO in a H_2 environment. The data for an air environment was not reported. In any event it can be inferred from the vacuum data and the shift of lattice parameter that there is an atmosphere effect. Perhaps the factor of 4 lower solubility in CO is reasonable. Another possible explanation is that a higher solubility exists at the forging temperature, but that $MgAl_2O_4$ was exsolved during furnace cooling. However, the coarse grain size with the longer diffusion distances makes this unlikely. There is also a possibility that the MgO solubility is somewhat lower than the 0.02 wt. % MgO estimated as there was microstructural evidence for $MgAl_2O_4$ segregation at the surface. This implies that some MgO was lost due to volatilization. Based on this discussion, the observed 0.02 wt. % MgO limit should be termed an "experimental concentration limit" applicable to forging Al_2O_3 at 1880°C in graphite dies. It is worth mentioning that 0.1 - 0.3 wt. % MgO is often added as a grain growth inhibitor in hot pressed or sintered Al_2O_3. This level appears too high by a significant margin and spinel phase should be observed.

Forging 1840 was analyzed for crystallographic texture. The inverse pole figure shown in Figure 8 demonstrates a marked preferred basal plane orientation, as has been observed previously for both flat and hemispherical forgings.[1] The shift from a smooth curve at ϕ = 39° is judged to be a result of the large grain size (33 μm). Eccentric peaks were noted in the diffractometer trace even using a $\frac{1}{3}$° rather than the normal 1° source slit. The R enhancement at ϕ = 0 and depression at ϕ = 90° is unquestionable evidence for strong crystallographic texture. Also shown in Figure 8 is the inverse pole figure for flat disc forging 47 and the error bars associated with the measurement. Data for forging 47 was averaged for three slow diffractometer scans on each of two specimen orientations relative to the X-ray beam. Thus, the error bars account for nonuniformity of
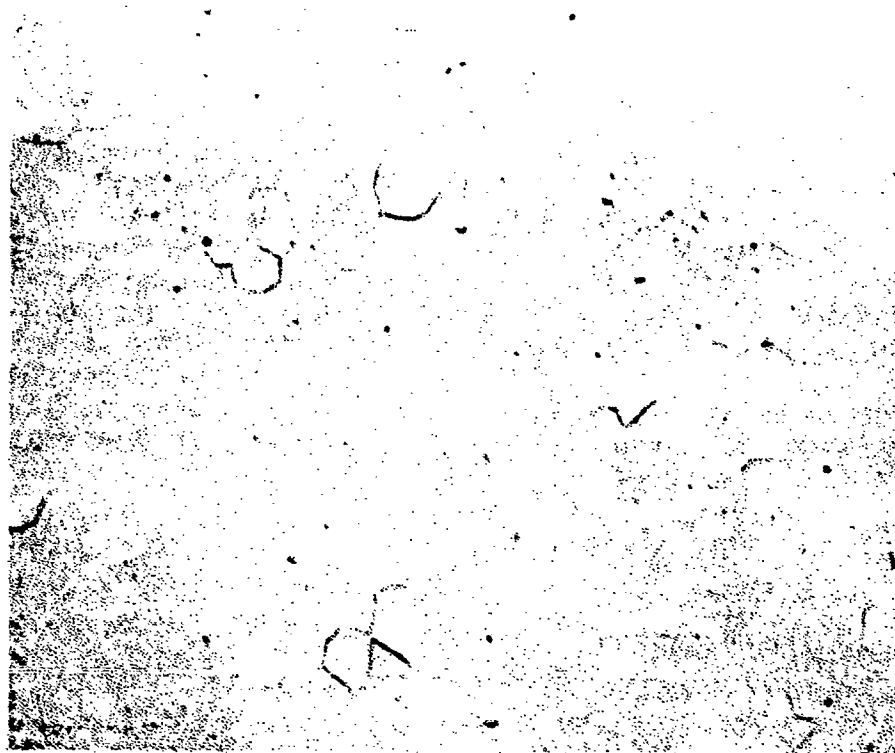
5703-3   250X

Figure 6.   Microstructure of Forging 1840 Showing Fully Dense Structure
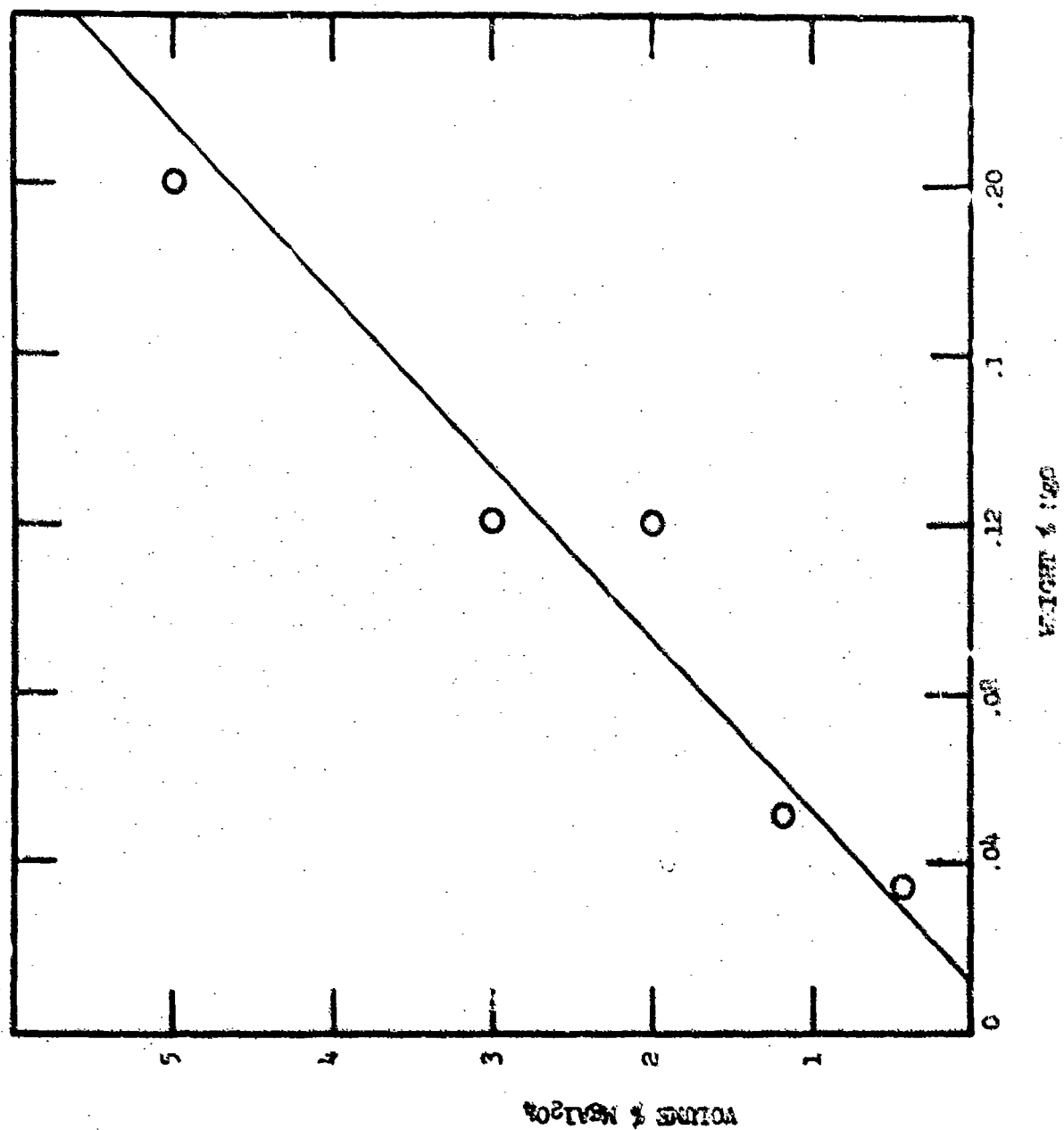and an Estimated 0.45 vol. % MgAl$_2$O$_4$.

Figure 1. Spinel Phase Detected Magnetostrictrally, as a Function of Starting Ag Concentration in Al_2O_3.
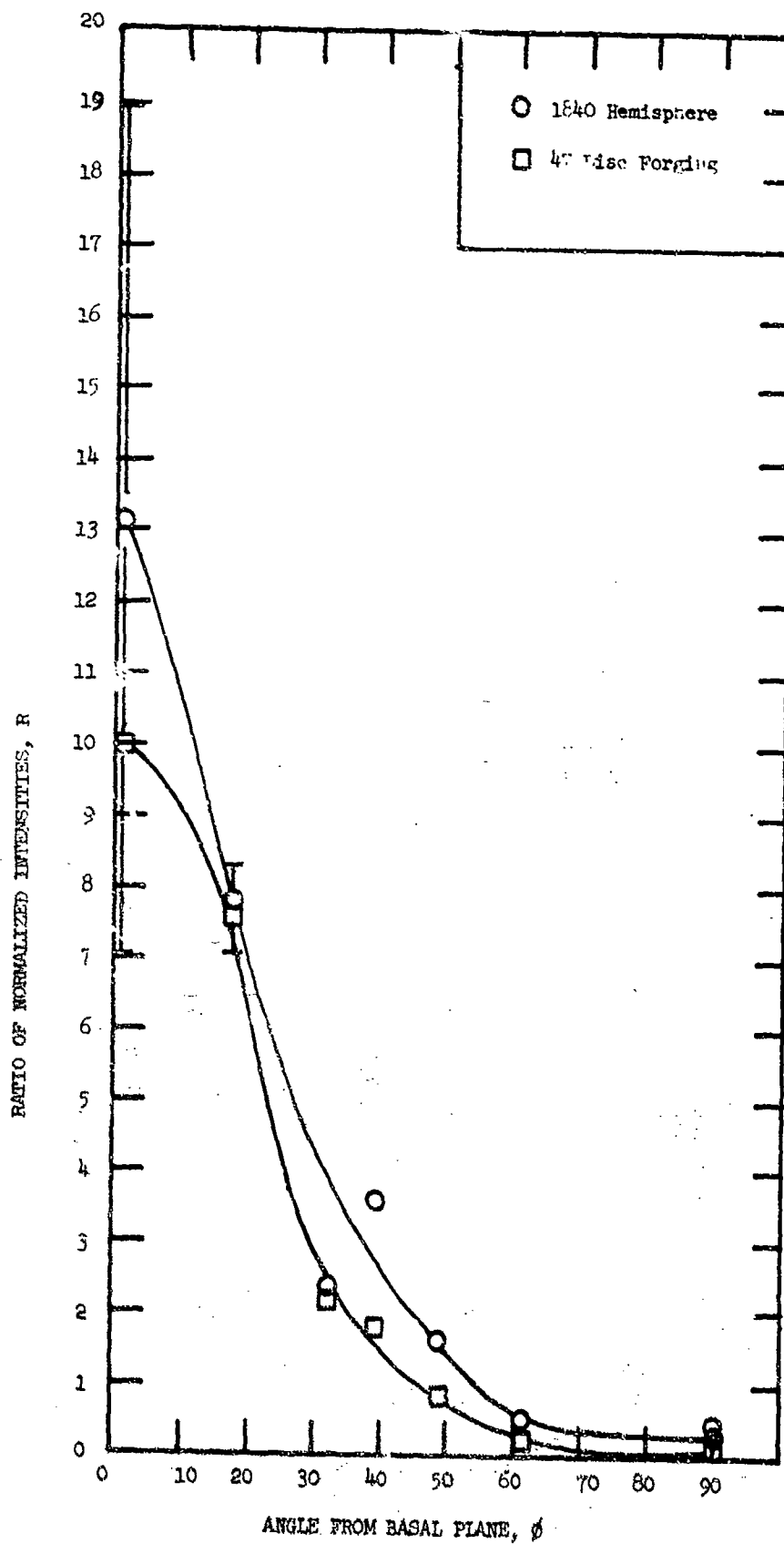
Figure 8. Inverse Pole Figure for Forged Hemisphere 1840 and Flat Disc Forging 47.

orientation, microstructure, taking a tangent to the forged surface, instrumental reproducibility and scale factor conversions. Unfortunately, the (006) reflection is one of the weakest in the Al_2O_3 structure, so the error bars are exceedingly large at $\emptyset_{001} = 0$. Better statistics were obtained for other reflections, thus it is possible to state that the disc forging had a stronger texture. The {0001} orientation has previously been accounted for as a result of rotation of the basal plane by a basal slip mechanism due to a superimposed bending moment. Diffusional and grain boundary sliding mechanisms probably account for the necessary accommodation to allow basal slip to continue without cavitation.

Transmission in the visible range has previously been reported.[1a] A 2 mm thick "c" direction sample exhibited 72% total and 49% in-line transmittance at 0.55 μm wavelength. These values were compared with a "very" transparent 1.3 mm thick sintered Lucalox specimen having 77% total and 15% in-line transmittance at 0.55 μm. The higher total transmittance for the slightly thinner Lucalox specimen indicates that the density of this specimen was indeed excellent and lends credence to the validity of comparing the in-line transmissivity of this sample with the forged Al_2O_3. The 35% higher in-line transmittance for the forged Al_2O_3 compared with the sintered Al_2O_3 was judged to be principally due to the reduced optical anisotropy resulting from the crystallographic texturing achieved in forging.

At larger wavelengths, the in-line transmission increases for both forged and sintered Al_2O_3. The fall off in transmission above 4.5 μm wavelength is from true absorption with the thicker sample falling off faster as expected from the relation

$$\frac{I}{I_o} = T = (1 - r)^2 \, e^{-x\alpha} \tag{1}$$

where I is the intensity of transmitted light, I_o is the intensity of the incident beam, T then becomes the fraction transmitted, r is the surface reflection coefficient, x is the thickness of the sample, and α is the absorption coefficient. The absorption coefficient for sapphire is between 0.02 mm^{-1} and 0.03 mm^{-1} at 4.5 μm wavelength and 0.19 mm^{-1} at 5.35 μm wavelength.[6,7]

The effect of thickness on transmission through forged Al_2O_3 at 4.5 μm wavelength is shown in Figure 9. A variety of disc and hemispherical forgings are plotted. The samples have varying densities, crystallographic orientation, and second phase content accounting for the scatter. The best fit gives a calculated absorption coefficient of 0.15 mm^{-1}. Since it is significantly higher than that for sapphire, the value is judged to be extrinsic and due to porosity, impurities, and second phase scattering centers. Grimm, Scott, and Sibold[8] measured an absorption coefficient of 0.3 mm^{-1} for 3.975 gm/cc or greater Lucalox at 4.5 μm wavelength. It is not clear that the lower absorption coefficient in forged Al_2O_3 can be attributed to the crystallographic orientation of the forged samples as previously discussed for measurement at 0.55 μm wavelength. Index of refraction measurements in the infrared report only the ordinary ray value[9] and no reference could be found for the extraordinary ray. A decrease in birefringence with increasing wavelength is one possible explanation for

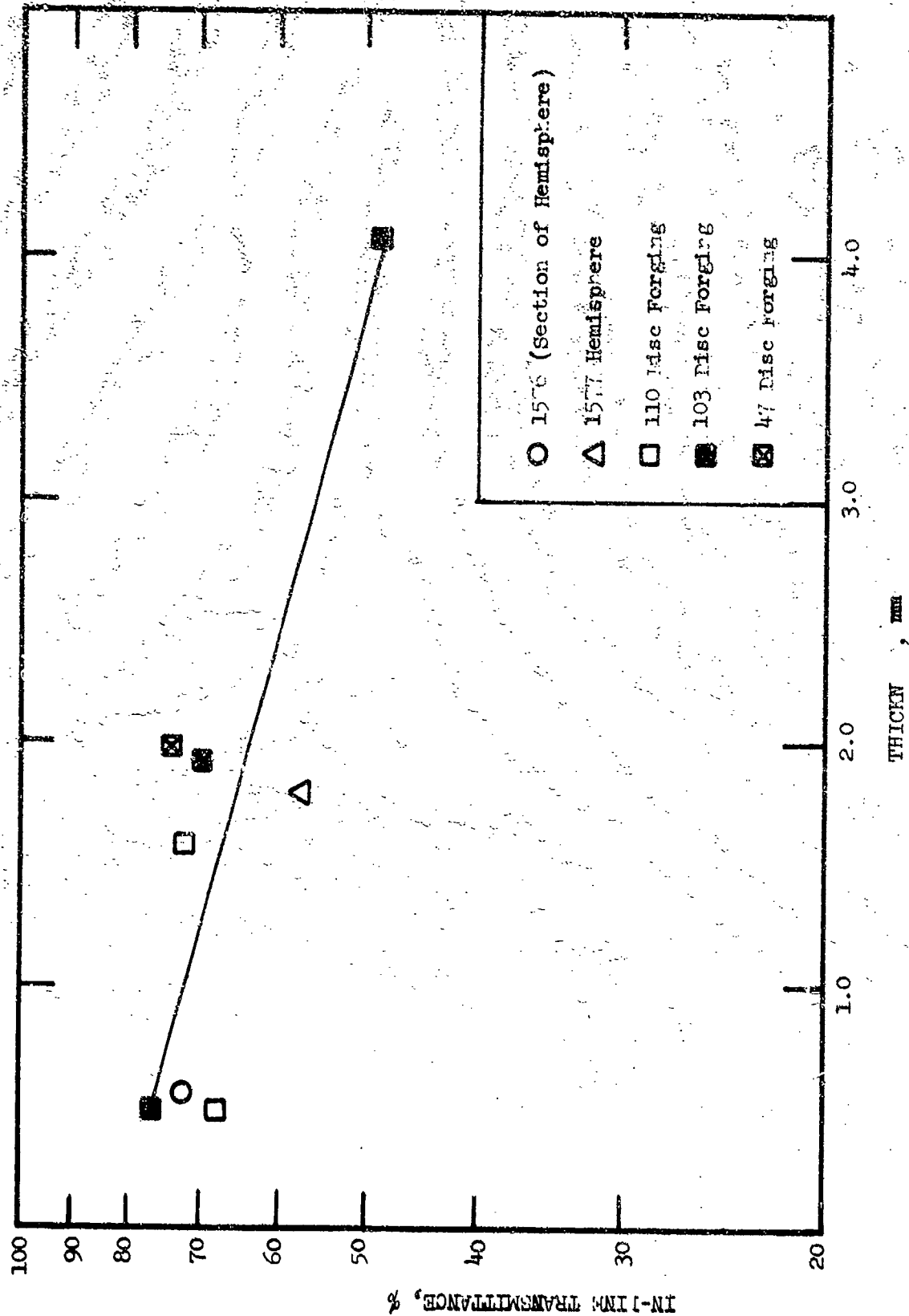Figure 9. Transmittance of Hemispheres and Disc Forging versus Thickness at 4.7 wavelength.

Legend:
- ○ 1576 (Section of Hemisphere)
- △ 1577 Hemisphere
- □ 110 Disc Forging
- ■ 103 Disc Forging
- ⊠ 47 Disc Forging

THICKN , mm

IN-LINE TRANSMITTANCE, %

increasing transmission from 0.8 to 4.5 μm wavelength for both forged alumina
and Lucalox. However, Grimm et al[8] contend that the decreasing absorption
from 3 to 4.5 μm wavelength was proportional to $1/\lambda^4$ and therefore supports
a small particle scattering model for the absorption or in-line loss coeffic-
ient in this wavelength region. This argument appears reasonable especially
in view of the fact that the absorption coefficient for both forged alumina
and Lucalox appear highly extrinsic when compared with the value for sapphire.
However, in view of the consistency of the birefringence-crystallographic
orientation model in explaining the optical data in the visible wavelength
range, the lower absorption coefficient at 4.5 μm for forged alumina than
randomly oriented Lucalox, the fact that similar quality starting powders
were used for specimen preparation, and that the microstructure of the
forged specimens were not highly perfect (spinel second phase), it appears
equally reasonable that a finite level of birefringence does exist at 4.5 μm
wavelength, and has the net result of allowing greater in-line transmission
for the oriented polycrystalline body.

G. Conclusions

1. The press forging process is capable of fabricating complete
    hemispheres having high in-line transmissivity.

2. Both cold press and sintered preforms can be employed. Cold
    pressed preforms exhibit greater accommodation, thus the fabrica-
    tion of a crack-free hemisphere is somewhat easier. Sintered
    preforms have to date always exhibited non-catastrophic rim
    cracks that occasionally extend from the skirt into the hemi-
    sphere. To date, sintered preforms have resulted in a higher
    density more transparent product.

3. It was shown that as little as 0.035 wt. % MgO addition results
    in 0.45 vol. % $MgAl_2O_4$ phase, and it is estimated that 0.015 wt.
    % MgO is the "experimental concentration limit."

4. An absorption coefficient of 0.15 mm^{-1} at 4.5 μm wavelength
    was found for forged Al_2O_3 which is about half of that for
    sintered Al_2O_3. This suggests that there may be a slight
    birefringence in the infrared region.

5. A preferred basal crystallographic texture was developed
    parallel to the hemisphere surface which was attributed to basal
    slip playing a strong role in the deformation process. The
    texture was slightly less than that achieved in one of the best
    flat disc forgings.

III. FLAWS IN ALUMINA AND THEIR EFFECT ON STRENGTH

A. General

Pears and Starrett[10] found an effect of specimen volume on the
strength of alumina of the type predicted by Weibull, but no single set of
Weibull constants could be found. Although many data points were eliminated
because of obvious flaws, microscopic flaws in the order of 1 to 50 grain

diameters in size may have contributed to the problem of defining a single set of Weibull parameters. Such a conclusion was reached in a previous report on this subject[1h] where microscopic flaws were correlated with strength in hot pressed Al_2O_3. Flaws were detected which reflected both a process origin and a raw material origin. Identifiable second phase inclusions were found both in the as-received powder and the hot pressed billets. Two billets were produced from one manufacturer's powder using different powder lots, but identical process conditions. The average microstructures were identical, but both the mechanical properties and flaw origin were quite different. Thus, it is clear that the problem of defining the strength of hot pressed Al_2O_3 by a single set of Weibull parameters was probably not within the limits of technology at the time this original work was completed. The question of whether or not it is within the current state of technology is appropriate and was considered in the current effort. This current work considered hot pressed alumina from two new powder sources rounding out consideration of the major vendors of hot pressing grade powder.

B. Powder Characterization

Powder selected for this program was supplied by two vendors previously used for many fabrication studies on moderately high purity Al_2O_3 with a specification of 99.98% pure and 0.3 micron particle size. Emission or mass spectrographic analy-'s of starting powders gives a very selective volume analysis which may o. may not be representative of the total batch. Further, an impurity particle or high concentration of solid solution impurities could be complet ly by-passed in the sample selection process. Therefore, Vendor II and Vendor III powder was subjected to a cutting and X-ray diffraction a alysis in addition to the standard emission spectrographic analysis. Vendor I powder was examined in detail in the previous report.[1h]

A vendor-supplied impurity analysis is reported in Table II. Both powders appear to be of high quality and easily fall within the purity specifications. Although Al_2O_3 solid solution solubility limits have not been determined for most of the elements listed, it is judged that the elements reported would all be within the solubility limit. The major problem with this type of analysis is that it is very selective. Only a few hundred milligrams are analyzed in any one determination making it quite possible to completely miss a discrete impurity particulate such as those described in the next section.

Two types of particle surveys were conducted. In the first analysis, ~ 3 gm of powder was extracted from a previously unopened container and surveyed under an optical stereomicroscope at 10-45X. Such an analysis on Vendor II powder resulted in 20 grey-black particles, one grey fiber, one straw-colored fiber, one clear rod, and 5 yellow-brown particles. The second technique consisted of preparing a slurry in a shallow dish, drying, and examining a 2 by 2 inch square area with the dish upside down using bottom lighting. In this way, semi-quantitative particulate impurity concentrations were conducted. These results are reported in Table III for both Vendor II and Vendor III powders. Both powders contain a large number of particulate impurities, but the powder from Vendor III exhibited only one type of impurity and about half the concentration of impurities compared with Vendor II. Based on depth of focus and a check of the powder

TABLE II

Emission Spectroscopy Analysis

	Concentration in ppmw	
	Vendor II	Vendor III
Si	25	30
Pb	ND	1
Fe	22	10
Mg	Tr	1
Ga	11	3
Ca	Tr	3
Cr	Tr	1

TABLE III

Quantitative Analysis of Particulate Contamination

in Alumina Powder

Supplier	Analysis Number	Black Particulates	Brown Particulates	Large Clear Particulates	Total
Vendor II	1	9	1		10
	2	3	2		5
	3	8		1	9
				Average	8
Vendor III	1	4			4
	2	4			4
				Average	4

density after drying, the volume of sampling was estimated as 0.258 cm^3.
This translates to 294 particles/cm^3 and 147 particles/cm^3 of dense material
for Vendor II's and III's powder, respectively. The average spacing between
particles would be 0.15 cm and 0.19 cm. These numbers probably have a
$\pm$ 200% accuracy, but even with this tolerance they reflect the fact that
particulate impurities can be closely spaced if they are allowed to become
incorporated in the final product.

Figures 10a and b illustrate a collection of the various impurities
in the two powders. These particulates were analyzed by X-ray diffraction
and are reported in Table IV. In addition, αFe_2O_3 was found in Vendor II
powder. The Fe and Al contamination must occur after calcination. The
αSiO_2 is probably from the fused SiO_2 calcining containers. Large αAl_2O_3
grains are probably residual powder which underwent many calcinations before
it became incorporated in this powder lot. The complex oxide may be a
result of a heavy impurity concentration which reacted with the Al_2O_3
during calcination, and the fiber obviously came from some powder handling
process.

C. General Defect Analysis

One hot pressed Al_2O_3 billet from each vendor's powder was
examined for defects by a variety of microscopy techniques to include
fractured chips containing flaws. An attempt has been made to categorize
the predominant defects.

1. Spherical Shade Zones

Defects in this category contained no obvious inclusions as
detailed by optical microscopy and were one of several shadings relative
to the matrix; light color spheres with no distinct boundary, dark color
spheres with no distinct boundary, and light spheres with a distinct ring
and halo effect. The former defects are illustrated in Figure 11 and appear
light in reflected light and dark in transmitted light. Most often they
blend with the matrix when observed at high magnification in reflected
light. X-ray and microprobe studies previously reported[14] indicated that
high impurity or grain growth inhibitor concentrations may be responsible
even though a distinct impurity phase could not be seen by the usual micro-
scopic techniques. For example, high concentrations of Si and C were found
by microprobe, and it was shown[14] that the reaction

$$SiO_2 + 4CO \longrightarrow SiC + 3CO_2$$

could occur under hot pressing conditions. Also, a minor concentration
of $MgAl_2O_4$ was observed in one such defect. It is judged that this type
of defect also arises from process related problems such as the formation
of a large agglomerate bridge which fails to break up during ball milling
or the addition of the grain growth inhibitor.

2. Second Phase Inclusion

Another class of defect which may be closely related to that
described above is the distinguishable second phase inclusion. Figure 12a
shows a lens shade zone surrounding a readily distinguishable second phase.
A similar appearing second phase was sectioned and revealed an inclusion

5654-4   150X

5654-1   20X

(a)

5654-2   150X

5680-1   (b)   100X
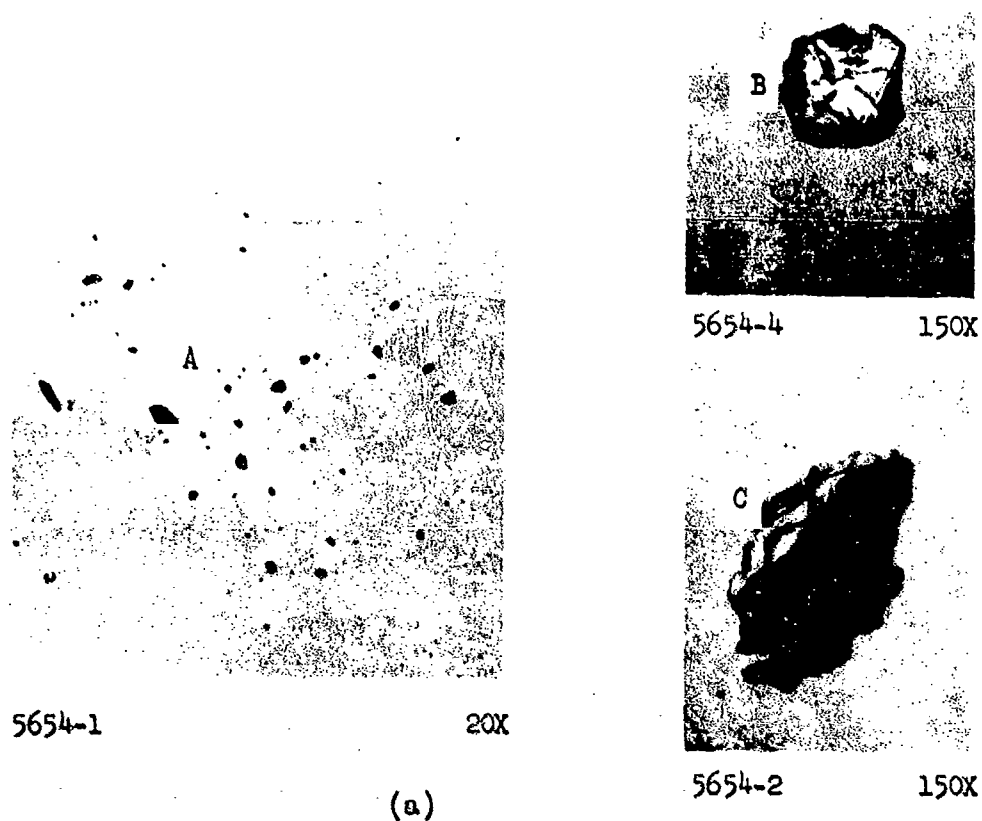
Figure 10. Impurity particulates found in (a) Vendor II, and (b) Vendor III
            alumina powder (letters reference particulates described in
            Table IV.)

TABLE IV

Identification of Particulates in Alumina Powder

Particle(s) in Figure 10	Size μm	Analysis
A	20-200	Single or compound rhombohedral metal oxide of either the Cr_2O_3-Al_2O_3 or $FeTiO_3$ ilmenite structure $a_o = 5.00$ Å, $C_o = 13.45$ Å.
B	150	One large and one small α Al_2O_3 grain.
C	200	α Fe
D	100	Organic fiber
E	60	Amorphous, shiney black, C?
F	30	One or two grains of α SiO_2
G	60	Al

5677-4A   50X

Figure 11.   Spherical shade zone in a billet fabricated from Vendor III powder.

5677-1)   (↑)   50X

5677-   (↑)   40X
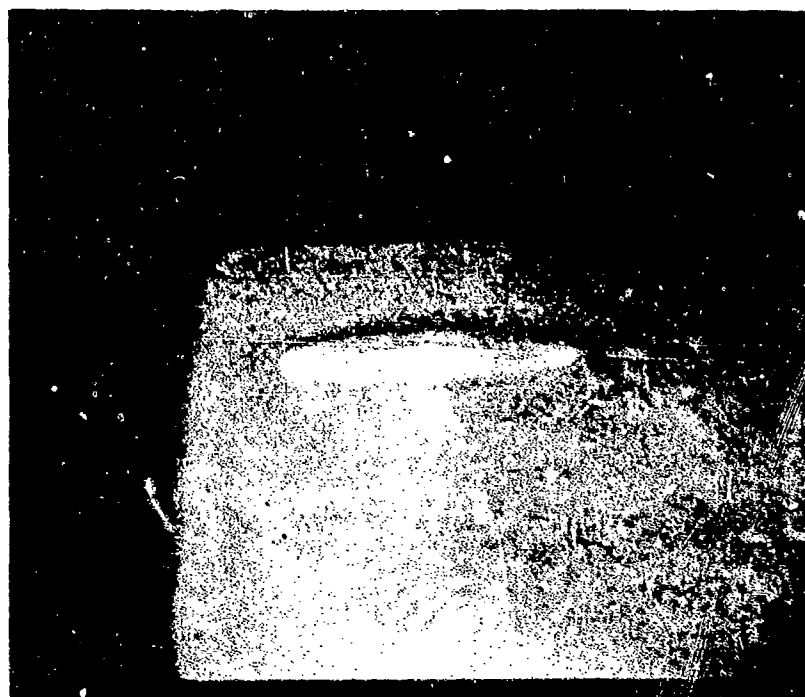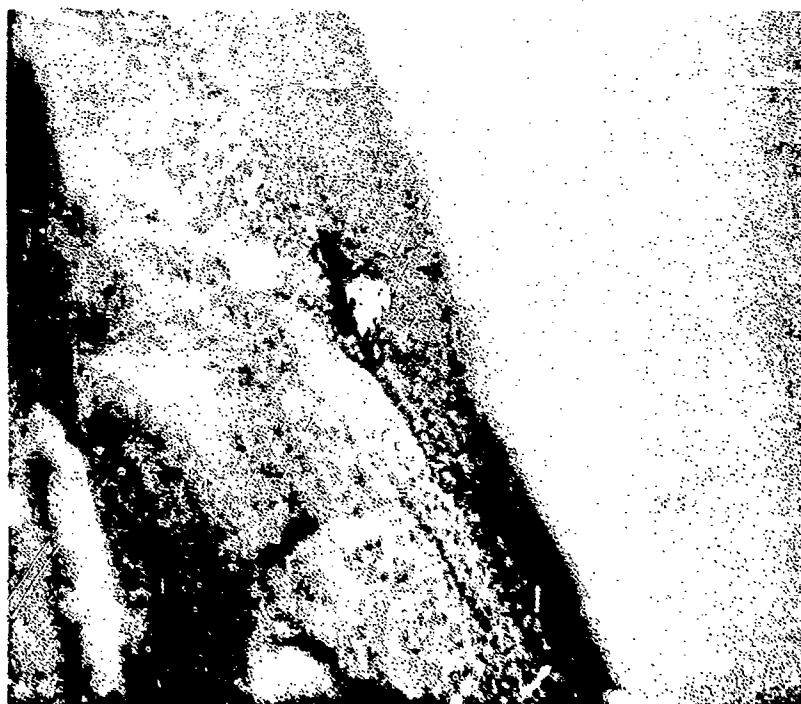
Figure 12. In......... , shown in (a) Lens Shaped before .... and (b) Metallic Flake Fractures ....

that was identified visually as a metal flake (Figure 12b), clearly a result of contamination. Figure 13 shows an inclusion with a fiber morphology. This inclusion did not exhibit a shade zone apparently indicating little chemical interaction with the matrix. It is thought that this inclusion is carbon in the "as-hot pressed" condition. The inclusion shown in Figure 14 was a dark green 100 μm transparent grain. This could be an alumina grain rich in impurities giving it a role similar to the exaggerated grain growth defect. However, it is included with this defect category as it probably has a raw material origin.

3. Exaggerated Grain Growth

This type of defect may be one of the more prominent defects in hot pressed Al_2O_3. Figure 15 illustrates a cluster of 20-30 μm grains. Grains half this size could still act as defects from a strength viewpoint and are not as easily found. Such defects could arise from inadequate mixing of the grain growth inhibitor, impurity promotion of grain growth, inclusion of a large Al_2O_3 grain in the powder (Figure 10), or perhaps just the statistical fluctuation of grain growth leading to the discontinuous process.

4. Fine Grain Region

No examples of this type of defect were found in Venders II and III materials. They may be present, however, so it is useful to categorize this defect which can be described as a zone of fine grains which appear to be poorly bonded and porous. The size of this defect is only several matrix grain diameters, thus it is much smaller than the spherical shade zones previously discussed. This fine grain defect is thought to be a pocket where agglomerate bridging has prevented adequate particle contact for solid state diffusion, sintering, and grain growth. There is no evidence that this defect has a chemical origin.

D. Hot Pressed Alumina for Testing

Billets for testing were fabricated for the test program from the powders already described. Details of the process and results are given in Table V. These conditions were selected to simulate sizes and processes used in the commercial production of hot pressed Al_2O_3. The data cannot be directly compared because of the different additive and process conditions. However, both billets are essentially single phase hot pressed Al_2O_3 with very similar microstructures, so on this basis a comparison was expected to yield new understanding. In addition, billets fabricated and tested in the previous period were directly comparable and will be the subject of some discussion.

E. Transverse Bend Strength and Flaw Analysis

Strength measurements were conducted in four point bending in ambient air with a relative humidity of 55%. The strain rate employed in testing was 6.9×10^{-5} sec^{-1}. The final finish on the specimen surface was obtained with a 400 grit wheel with the grinding direction parallel to

5675-1   135X

Figure 13. Fiber inclusion in billet fabricated from Vendor II material.

5677-8   40X

Figure 14. Dark grey or large single grain in matrix of Vendor III Material.

5677   160X

Figure 15.   Cluster of 20-30 um grains in material fabricated from
             Vendor III material.

TABLE V

Hot Pressed Alumina for Mechanical Test Program

Billet Number	Density gm/cc	Grain Size microns	Powder	Additive wt. %	Pressing Atmosphere
1118	3.979	2.9	Vendor II	0.1 MgO	Argon-Vacuum
459	3.986	1.9	Vendor III	0.2 MgO 0.1 NiO	Ambient

the specimen axis.

All testing was conducted in a ball bearing and stainless steel test fixture designed to reduce knife edge concentration and frictional effects. Consideration was also given to the shifting of the point of tangency at the load and support points. Vrooman and Ritter[11] have shown this to be a serious problem at high deflections, requiring a numerical analysis to obtain corrected stresses. The error in stress for the fixture employ i was calculated to be 0.025% at 100,000 psi. At this level and with the standard deviations usually found in Al_2O_3 testing, it was considered unnecessary to employ the numerical analysis. Shand[12] has discussed the interpretation of fracture features on glass to include mirror region of smooth crack extension from a flaw, crack branching, and interaction of the crack front with stress waves reflected from nearby surfaces to form Wallner lines. Kirchner et al[13] recently demonstrated that these regions may be identified in polycrystalline Al_2O_3 and are useful in some cases to find the fracture origin. Further, fracture origins could be located in several of their bars. Similar techniques were employed in this study.

Bend strengths are reported in Table VI along with the results of a detailed flaw analysis employing a combination of stereo and reflected light microscopy techniques as well as electron microscopy techniques. These results are summarized in Table VII.

Six liquid N_2 tests were conducted on billet 1118 N_2 to gain a measure of the absence of stress corrosion on critical flaws. The average strength of this specimen group was 50% higher than the specimens tested in an ambient atmosphere. The spread is perhaps 10-20% higher than normally observed[14] for a difference in the two types of tests. The direction of the shift and general levels of strength are within reason. The implications of the flaw analysis will be discussed in a subsequent section.

Potential difficulties in the testing of square cross section bend bars can arise due to a non-uniform cross section. Knife edge stress concentrations and torsional moments giving a complex biaxial stress condition are the two most likely difficulties. The severity of this problem in terms of readily obtainable machine tolerance is not well known. After the first nine (9) specimens of billet 1118 were treated, it was noted that the machining tolerance and squareness was not up to the normal standards.

TABLE VI

Fracture Strength and Flaw Analysis

Specimen and Test Condition	Bend Strength Kpsi	Observations
As Machined + 23°C		
459-1	72.9	Fracture origin at large grains
459-2	70.2	Fracture origin at large grains
459-3	55.9	Particulate inclusion at fracture origins
459-4	46.1	Fracture origin at corner. No flaw located.
459-5	80.1	Fracture origin at one large grain
459-6	57.5	Fracture origin at large grains
459-7	56.6	Fracture origin located. No flaw located.
459-8	60.4	Fracture origin at large grains around a defect.
Average	62.5 ± 9.94	
As Machined + 23°C		
1118-1	58.8	Black inclusion at fracture origin.
1118-2	58.0	Vertical surface scratch at fracture origin.
1118-3	61.1	Fracture origin at fine grain patch.
1118-4	66.7	Black inclusion at fracture origin.
1118-5	64.0	Black inclusion at fracture origin.
1118-6	67.1	Either black inclusion or large grain at fracture origin
1118-7	54.7	Corner origin - no flaw located.
1118-8	65.1	Black inclusion at fracture origin.
1118-9	68.7	Possible large grain at fracture origin
Average	62.7 ± 4.89	

TABLE VI (Cont'd)

Fracture Strength and Flaw Analysis

Specimen	Bend Strength Kpsi	Observations
Remachined + 23°C		
1118-10	71.7	Corner origin - no flaw located
1118-11	48.1	Fine grain patch at fracture origin
1118-12	64.9	Either black inclusion or 5-10 μm grain as fracture origin
	61.2	
Remachined - 196°C		
1118-13	80.5	Black inclusion at fracture origin
1118-14	102.5	Black inclusion 100 μin from tensile surface - possible fracture origin.
1118-15	94.5	No obvious flaw at fracture origin
1118-16	101.2	No obvious flaw at fracture origin
1118-17	92.1	Possible 10 μm grains at fracture origin
1118-18	72.2	Possible 10 μm grains at fracture origin
	Average-90.6	

TABLE VII

Summary of Flaw Analysis

Billet	No. of Tests	No Flaw Detected	Large Grains	Particulate Inclusion	Machining Error	Fine Grain Region
459	8	2	5	1		
Average Strength, Ksi	62.5	51.3	68.2	55.9		
23°C-1118	12	1	1	6	2	2
Average Strength, Ksi	62.3	71.7	68.7	64.4	54.7	54.6
-190°C-1118	6	2	2	2		
Average Strength, Ksi	90.6	97.8	82.1	91.5		
Frequency of Occurrence in Total Testing, %		19.2	30.8	34.6	7.7	7.7

Therefore, it was decided to resurface the remaining nine (9) specimens for a check on the severity of the "out of squareness" problem as well as other testing on the task. The task results on this subject are given in Table VIII. The average strengths are essentially equal for the two groups indicating that either both groups are within or out of the necessary tolerance for these problems. Fracture origins were found on all the specimens and in every case but one the fracture occurred at a flaw. Several of the flaws were near a corner, but the majority were at least $\frac{1}{4}$ of the way in from a corner. The one specimen where a flaw could not be found had a corner fracture and also exhibited the lowest strength of the entire group (54.7 kpsi). This specimen also showed the greatest thickness variation (0.0008 inch) and a side to side variation that was on the high side (0.0003 inch), but not the highest of the "initial machining" group. Based on these observations, it was concluded that both groups on the average are within the necessary tolerance to avoid serious knife edge or biaxial stress concentration, but that such problems begin to affect results when the thickness tolerance exceeds about 0.0005 inch.

It was interesting to note in Table VII that each billet possessed a dominant but different defect. Figure 16a illustrates a low magnification view of a specimen 459-6 having a large grain fracture origin, the major defect for this billet. A higher magnification view is shown in Figure 16b where it is quite clear that a cluster of grains 5-10X the nominal grain size was the critical flaw for failure at 57.5 kpsi.

Only one specimen from billet 459 exhibited a critical flaw associated with a particulate inclusion. A low and high magnification view of this specimen, 459-3, is shown in Figure 17. The semicircular flat region of Figure 17b is judged to be the classic mirror region of brittle fraction. This feature is often seen on glass, but has also been observed previously on hot pressed Al_2O_3.[1h,13] In the center of the mirror is a 20 μm long rod or plate shaped particulate impurity that is thought to be the critical flaw for failure at 55.9 kpsi. The close proximity of this flaw to the tensile edge results in a calculated stress of 5.5 kpsi at the upper tip of the flaw. Integrated secondary X-ray emission counting was performed on the region within the mirror and compared with the matrix. No evidence was obtained for an impurity concentration in this region, thus it is possible that the nature of the flaw has been improperly identified. It is also possible that the impurity particulate was lost or on the opposite side of the fracture. Thus, the authors will rest on their analysis which is based mainly on microstructure consideration.

Figure 18 illustrates a billet 459 fracture origin where the cluster of large grains surrounds an oblong zone. It is thought that an impurity particle was at the center of the oblong zone and was responsible for the entire microstructural anomaly. It is not clear whether the rather porous structure of the oblong zone or whether one of the large grains acted as the fracture nucleus at 65.1 kpsi.

The strength of billet 1118 was dominated by included particulate impurities. Figure 19 illustrates a low and high magnification view of one specimen whose strength was controlled by the inclusion. Failure was near a corner of the specimen. Stereomicroscopic examination conclusively

TABLE VIII

Dependence of Strength of Alumina on Specimen Tolerance

Condition	No. of Specimens	Average Width Variation Inches	Average Thickness Variation Inches	Average Side to Side Thickness Variation Inches	Average Strength Kpsi
Initial Machining	9	0.0003	0.0005	0.0003	62.7 ± 4.9?
Remachined	3	0.0003 (not touched)	0.0001	0.0001	51.2
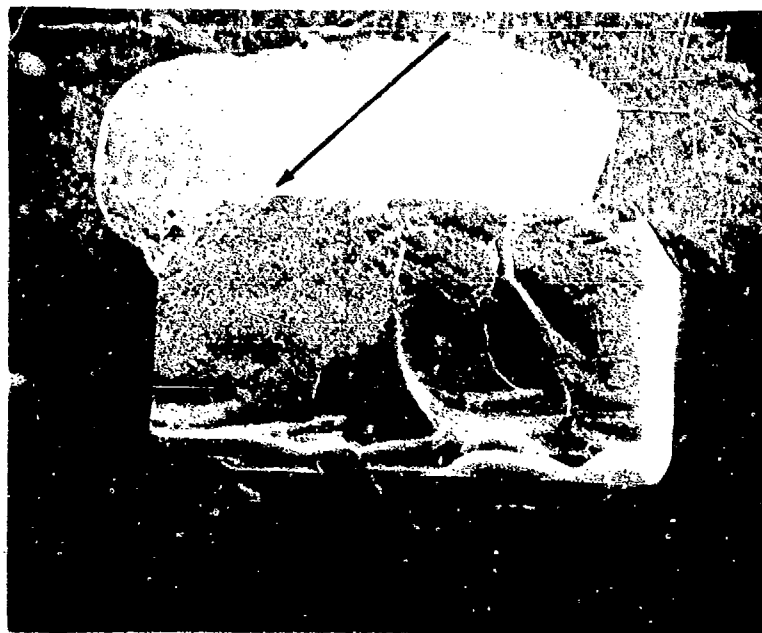
4   (a)   5X
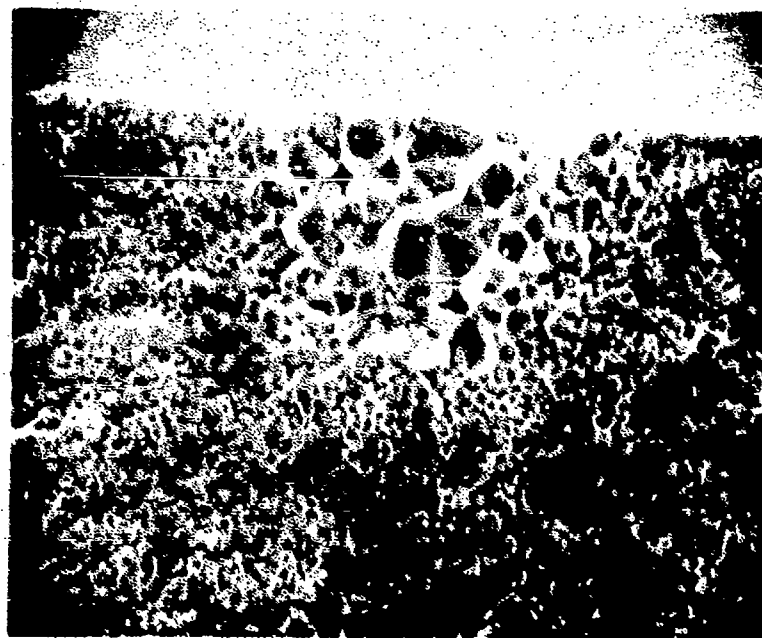
7   (b)   720X

Figure 16. Specimen 494-6 showing (a) fracture face and origin (arrow), and (b) critical defect to be cluster of large grains.

1   (a)   15X
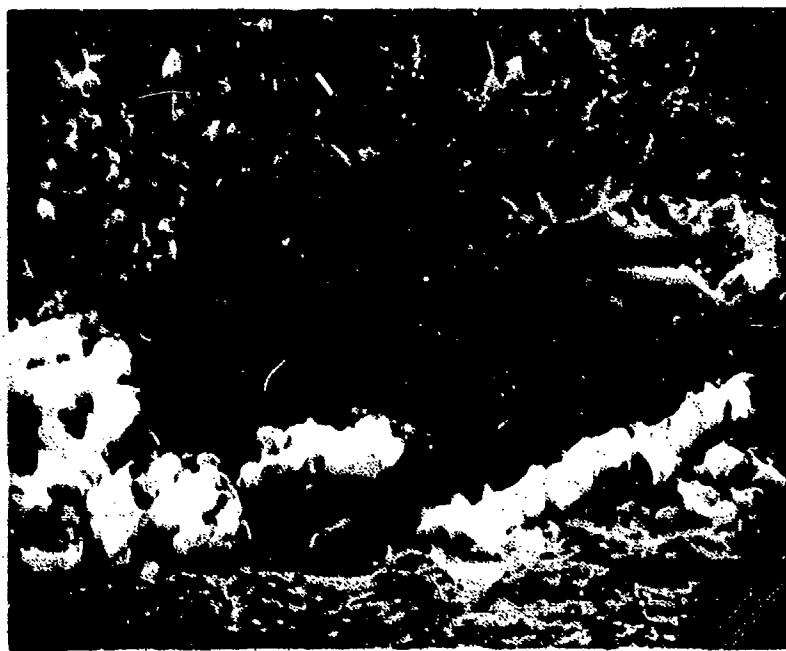
3   (b)   1500X

Figure 17. Bend specimen 459-3 showing (a) fracture origin, and (b) particulate impurity in spherical shade zone.
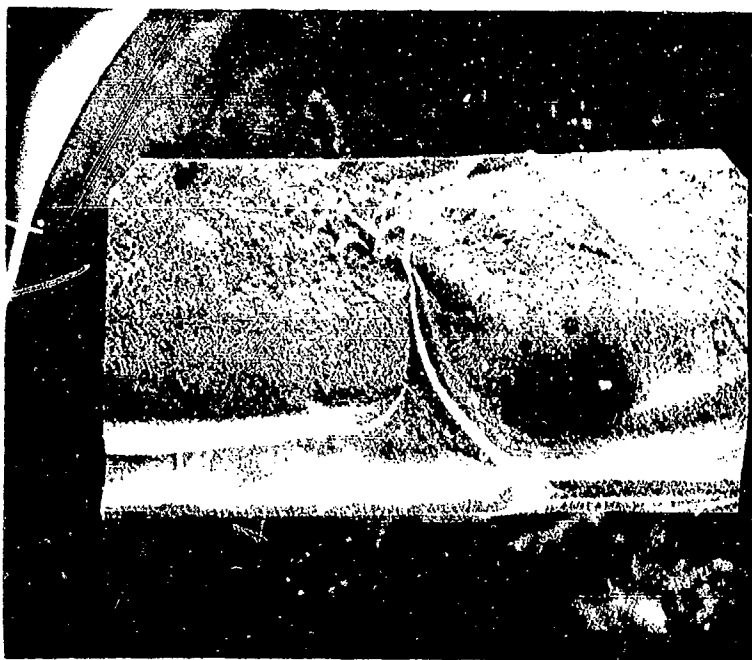
24   (a)   18X
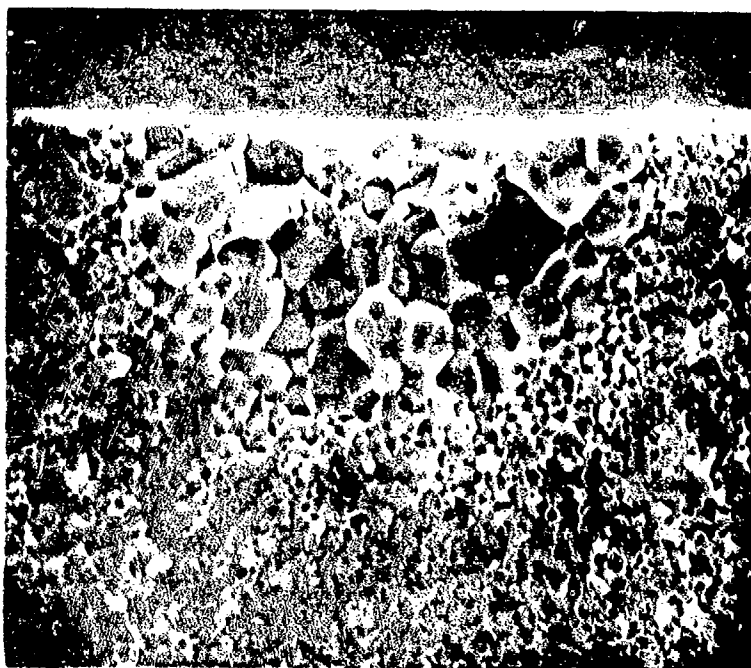
25   (b)   900X

Figure 18. Specimen 459-8 showing (a) fracture face and origin (arrow), and (b) critical defect to be large grains surrounding oblong impurity zone.

12   (a)   14X

13   (b)   365X

Figure 19.   Specimen 1118-1 showing (a) fracture face and corner origin (arrow), and (b) mirror surrounding defect (arrow) and fracture origin.
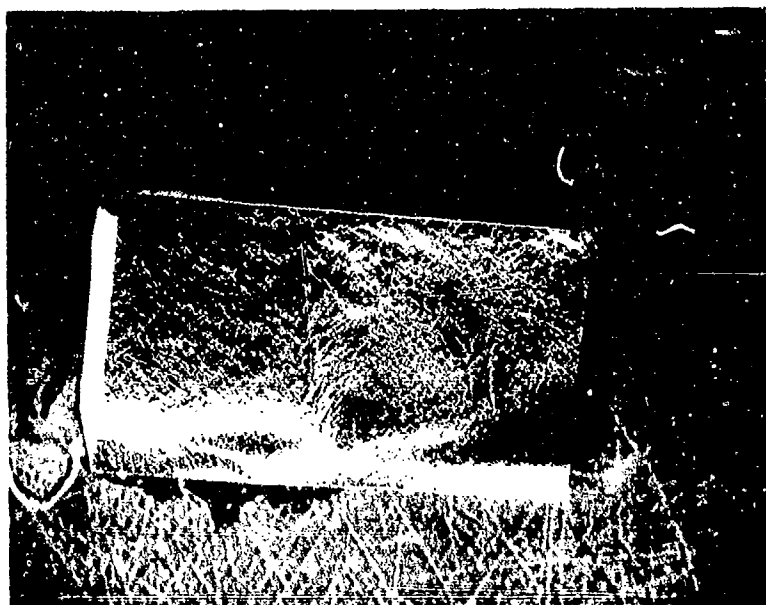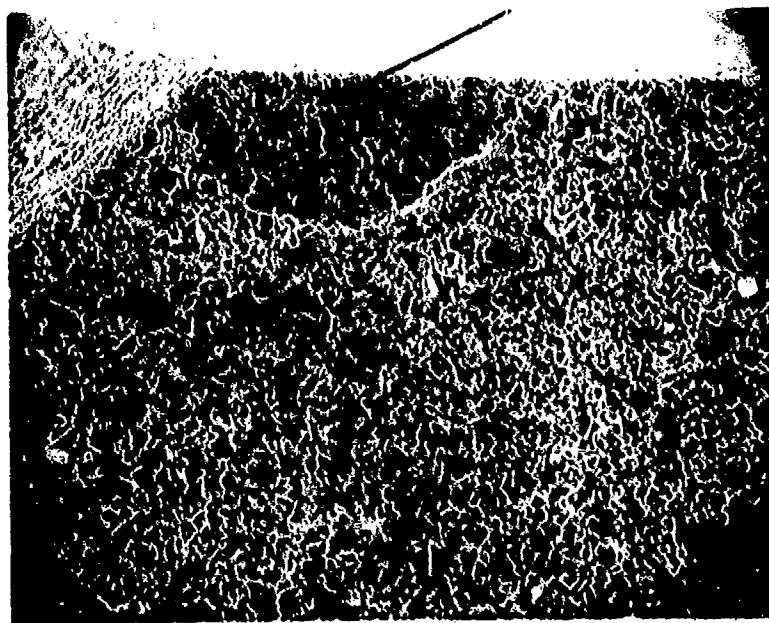
proved that a black impurity particulate was in the position designated
by the arrow of Figure 19b. The semicircular zone whose origin appears to
be at the arrow in all probability is the fracture mirror referred to earlier.
In several cases, black impurity particulates were found on the fracture face
and judging from the crack pattern, they were not the critical flaw for
specimen failure. In all cases the particulates were some distance away
from the tensile surface. A black impurity particulate is shown more clearly
in Figure 20 which is of specimen 1118-13.

The fracture of specimen 1118-9 at 68.7 kpsi was attributed to a
possible large grain. Figure 21 illustrates the fracture face and fracture
origin zone. There are several 8-10 μm grains near the tensile surface
which could be the critical flaws. This case is illustrated because it
demonstrates that the analysis is subjective and that seemingly rather minor
deviations from the average 2-3 μm grain size can in all probability act
as strength limiting features. This type of defect is expected to be the
most difficult to control and eliminate in the development of a better
material.

Specimen 1118-2 showed a clear fracture origin as illustrated in
Figure 22a. A shallow (5 μm) scratch parallel to the specimen axis was
noted. Also some 30 μm in form the tensile surface there were a number of
5 to 10 μm grains. It is not possible to state with confidence which is
the critical flaw. However, since the 5 to 10 μm grains are noted else-
where along the tensile surface of the bar, the scratch is suspected as the
fracture origin. The scratch itself does not appear sharp enough to act as
a critical flaw, thus it is suspected that damage caused by the scratch may
have caused nucleation of the crack. This damage might include dislocation
structures of the type observed by Hockey[15]. Rice and Becher[16] have noted
that horizontal scratches can act as crack nuclei and the authors previously[14]
found an angled scratch as a fracture origin. This may be the first
documented example of a parallel scratch as the fracture origin.

F. Discussion

The analysis of powders from two previously unopened containers
demonstrated that particulate impurities were prevalent in both grades.
This, together with the results previously reported, indicates that three
major suppliers of nominally 99.97% Al_2O_3 have a particulate contaminat'on
problem. A tentative grading of the powders based on the size and concentra-
tion of particulate impurities is Vendors I, II, and III in order of
decreasing particulate contaminatior. The impurity particulates appear to
average ~60 μm and can range in size up to 200 μm, which, of course, makes
them ready sources of flaws and failure in the final product. The produc-
tion of high quality Al_2O_3 bodies will require either finding a source of
inclusion-free Al_2O_3 powder, learning to clean powders, or encouraging the
present manufacturers to exercise scrupulous care in powder production.
This is a problem that must be common to all users of high quality Al_2O_3,
consequently it is expected that there would be great interest in securing
a successful solution.

Inclusions can be introduced during consolidation processing.
Examples of this have not been clearly defined during this study, but
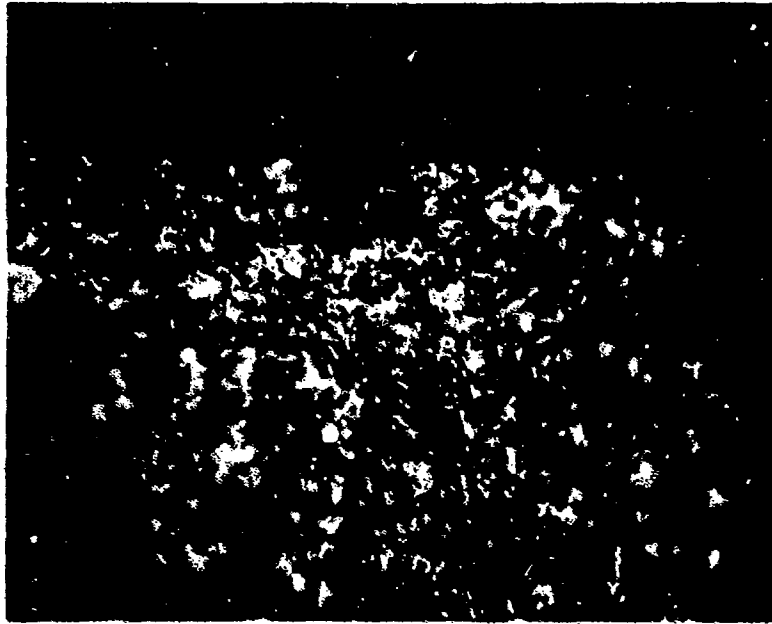
5762-2   250X

Figure 20.   Specimen 1118-13 showing black impurity particulate
             as fracture origin.

15   (a)   20X
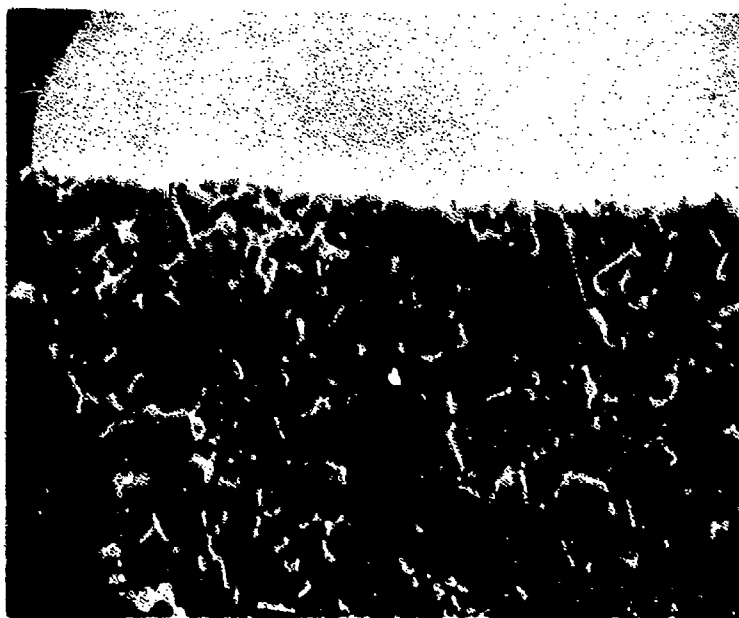
16   (b)   1000X

Figure 21. Specimen 1118-9 showing (a) fracture face and origin (arrow), and (b) structure at origin with possible critical flaws (10 μm grains) denoted.

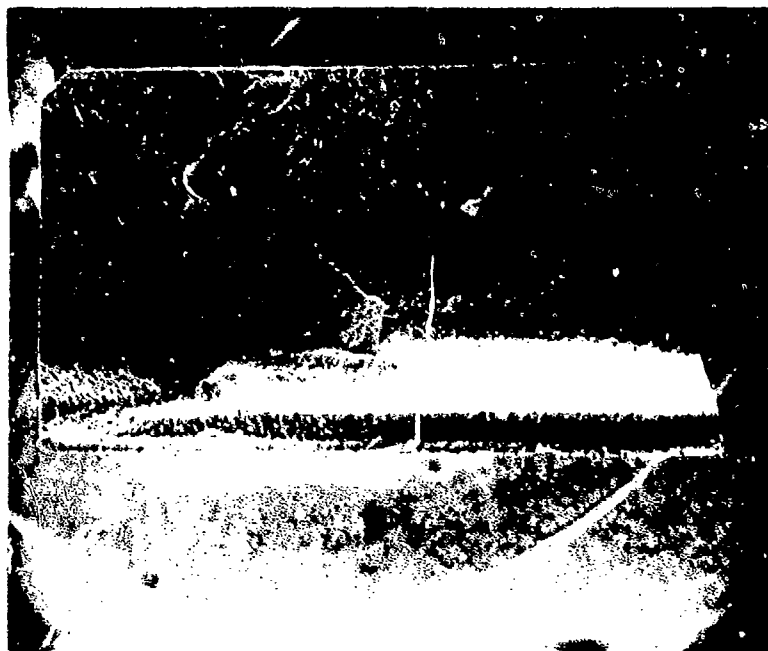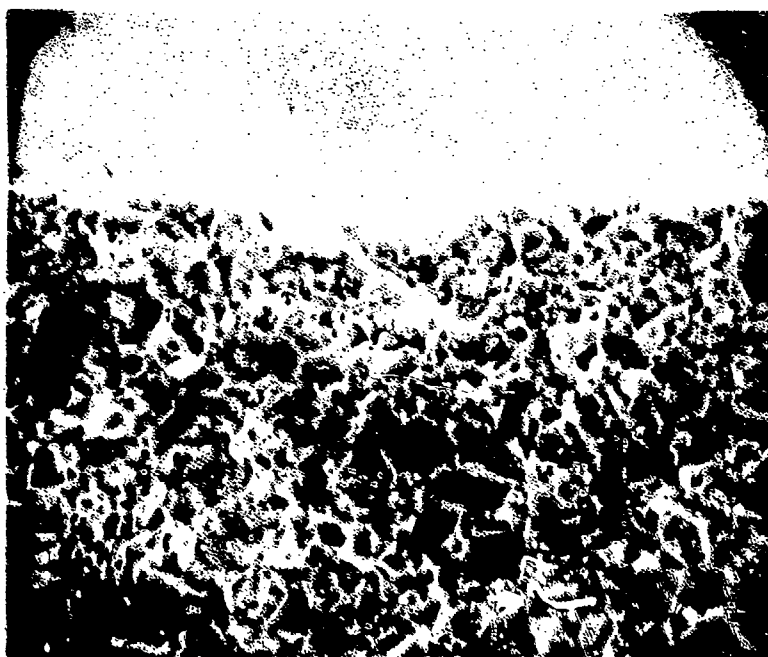8   (a)   15X

9   (b)   100X

Figure 22. Specimen 1118-2 showing (a) fracture face and origin (arrow), and (b) scratch parallel to axis of bar to be fracture origin.

previous work in hot pressing Al_2O_3 has shown the necessity of establishing procedures for eliminating particulate carbon as an in-process inclusion.

In terms of the generalized defects observed in hot pressed billets, the special shade zone is the least well understood, and may be of several origins. One such origin is thought to be an impurity particulate which reacts during pressing to affect a spherical zone around it. The other cause may be agglomerate bridging forming a slightly higher porosity nest. No examples of this defect as a fracture origin were encountered in the mechanical testing. These defects were widely spaced reducing the probability of them being in the zone of maximum stress. This does not mean that such defects can be ignored or minimized as applications such as gas bearings and substrates require highly perfect defect-free surfaces.

Second phase inclusions can act as major strength limiting defects. Some of the defects found both in the powders and billets range up to 200 μm in size. Many were in the 20 μm to 60 μm range, which is still apparently too large. Ball milling the powder is thought to be beneficial. This reduces the particle size of inclusion contaminants and uniformly distributes the grain growth inhibitor. It is thought that a finely divided SiO_2 will react to form $2SiO_2 \cdot 3Al_2O_3$ as a thin grain boundary second phase which would be preferred over a large α-quartz inclusion. The grain boundary phase would still represent a source of weakness and corrosion susceptibility as the grain to grain bond strength would be reduced over a pure Al_2O_3 system. The ball milling employed was apparently not sufficient to completely reduce the impurities to a grain boundary phase. Furthermore, it is not clear whether or not this approach is feasible. However, it is thought that further advances can be made both by the manufacturers of powder and in processing.

Exaggerated grain growth may result from one of three causes. Since MgO is added as a grain growth inhibitor, one explanation is that the MgO was not uniformly distributed and that the grains grew by the classic exaggerated grain growth mechanism. The fabrication process included a 16-hour wet ball milling as the manner of mixing the MgO, which is usually considered to be a very efficient and thorough manner of mixing. A second possible explanation is that impurities were clustered in a local volume and promoted grain growth to the point where exaggerated grain growth took over, resulting in the very large grains. Large colored grains of αAl_2O_3 have been found and are taken as evidence for impurity promoted grain growth. A third possibility is that large αAl_2O_3 grains were present in the powder (Figure 10) and acted as nuclei for further exaggerated growth.

The two billets tested in this period had essentially equal strengths. One was vacuum pressed (1118) and the other ambient pressed. Also, billet 1118 had a grain size about 1 μm larger than No. 459. Normally the vacuum pressing results in stronger material as does going to smaller grain sizes provided density remains constant. The billets in question varied in such a way that the atmosphere and grain size parameters may have cancelled, resulting in billets of equal strength. Such a line of reasoning probably would have been acceptable if the fracture origins had not been examined in detail. Having done so it is possible to emphatically state that flaws larger than the matrix grain size <u>controlled</u> the recorded fracture stresses

of the billets in question. This being true, there is no reason to expect
average strengths from these billets to fit on any strength-grain size
plot in a way that could be used in any mechanistic arrangement.

Several specimens where the flaw size was accurately measured are
plotted in Figure 23 as strength versus flaw size. Also plotted are
several data points from the previous work[1h] and three commonly referenced[14,17,18]
strength versus grain size curves where the grain intercept times 1.5 was
considered the flaw size. There is perhaps more scatter in the data than
sometimes observed in strength-grain size studies. This is in part due to
the fact that individual data points are plotted rather than averaged data.
The point to be made, however, is that when a best fit line is drawn through
the data, a line very close to the hot pressed Al₂O₃ curve of Spriggs,
Mitchell, and Vasilos[18] is generated. This lends credence to the validity
of plotting the strength data versus flaw size rather than average matrix
grain size. Another way of viewing the agreement is that it lends support
to the data of Spriggs et al suggesting that the matrix grains rather than
flaws were the crack origins in this work.

This identical strength data is plotted versus the inverse square
root of grain or flaw size in Figure 24. Also included in this plot are
the average billet strengths versus matrix grain size. A straight line
extrapolating to the origin is expected if the behavior follows the
Griffith relation

$$\sigma_f = \left(\frac{2E\gamma}{\pi C}\right)^{\frac{1}{2}}$$

where σ_f is the fracture stress, E the elastic modulus, γ the fracture
surface energy, and C the half length of the elliptical cross section of
the crack. Alternately a two branch curve is interpreted to follow the
Petch relation of the form

$$\sigma_f = N(\sigma_y) + KG^{-\frac{1}{2}}$$

where $N(\sigma_y)$ is a constant related to the yield stress, K is a constant,
and G is the grain size. In addition to yield or micro-yield phenomena,
Rice[19] has attributed non-zero intercepts to thermal expansion anisotropy
and elastic anisotropies. Figure 24 shows that the Griffith equation (3)
is followed if the flaw size is plotted. The average billet strengths and
average grain sizes fall off the curve and near the two branch curve of
the data of Spriggs et al[18] as analyzed by Carniglia[20]. It has been shown
in this study that "average grains" are not flaw origins; consequently,
plotting the data this way has no relation to the actual mechanism. It is
suggested that the data of Spriggs et al[18] is also subject to the same
restrictions since their material was fabricated from an earlier version of
one of the powders studied in this project. Thus, branching of the Petch
plot for Al₂O₃ appears to be caused by increasing flaw to grain size ratios
with decreasing grain size rather than plasticity. This possible explanation
has been discussed previously by the authors[1h] and by Rice.[19]

The finding that the flaws larger than the matrix grains can be
responsible for Petch plots that appear to follow the equation points out
a difficulty and pit fall in analyzing data generated by others particularly
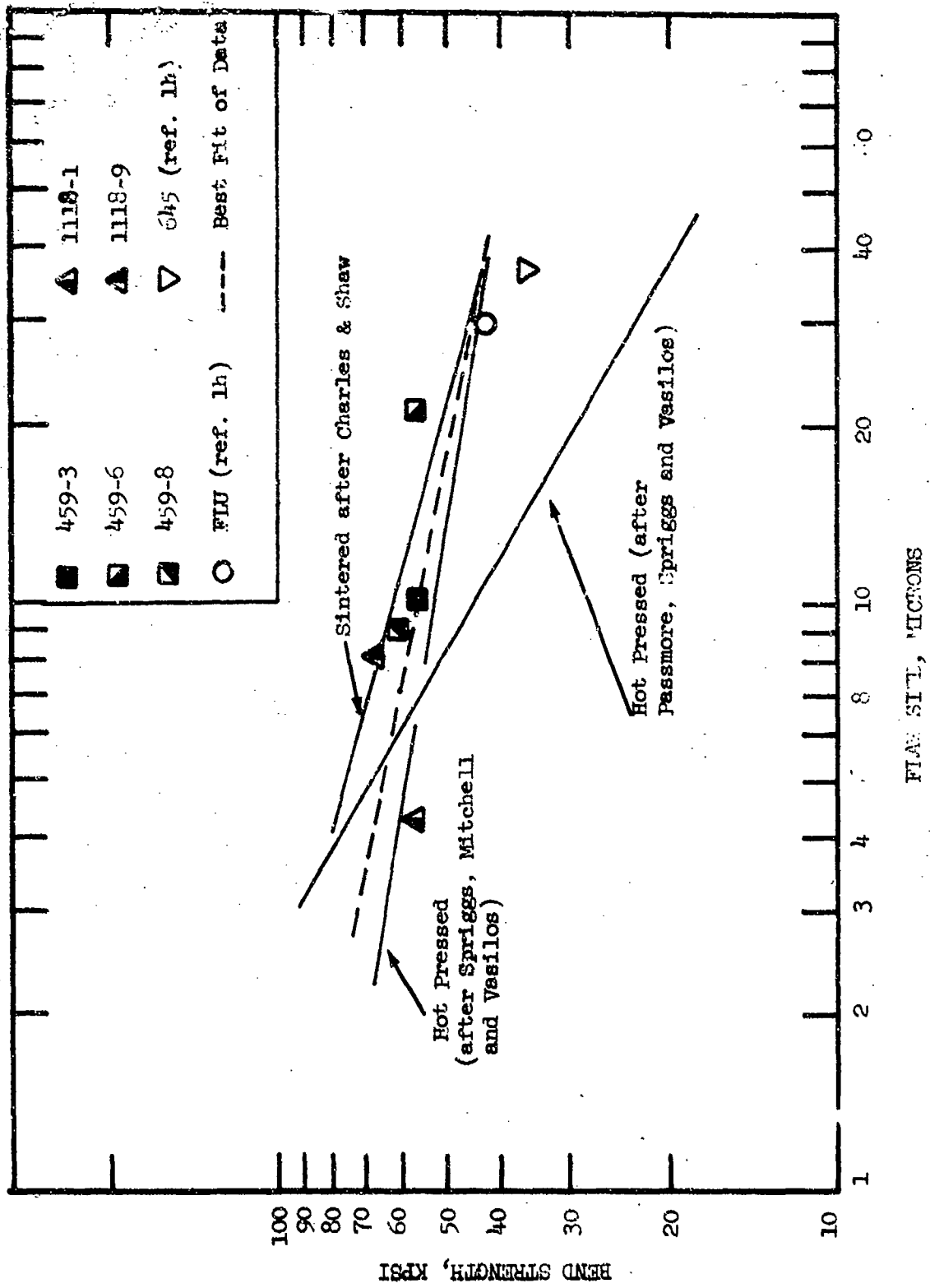for fine grain materials. Unless the fracture surfaces are examined and

Figure 23. Room Temperature Bend Strength Versus Flaw Size Compared with Literature Grain Size Data.
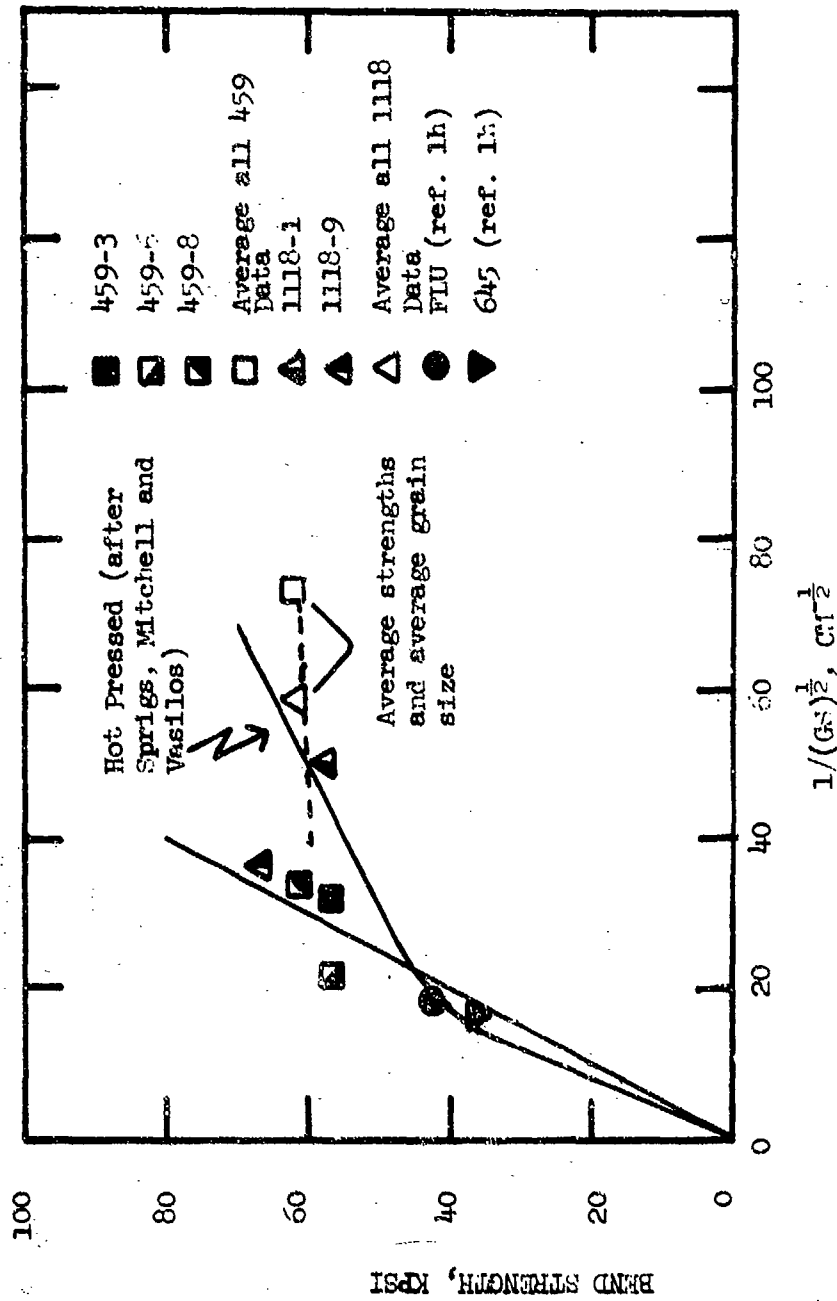
Figure 24. Room Temperature Bend Strength Versus Square Root of Inverse Grain or Flaw Size.

found free of flaws larger than the matrix grain size (the authors suspect
that few such cases will be found at grain sizes under 10 μm) further analy-
sis and interpretation does not appear warranted. Rice[19] has taken the
approach of emphasizing the large grains in his grain size measurement; this
appears quite correct in cases where impurity or porosity related flaws are
absent.

The results of this study as well as the previous effort in this area
indicate that care must be exercised in performing a Weibull analysis on
ceramics. Certainly in the case of hot pressed Al_2O_3 difficulty could be
expected if different powder vendors were used to supply powder for the
billets under consideration. Evidence was obtained[14] for a lot to lot
variation in particulate analysis and final properties from one vendor's
powder. Consequently, at this state of the art the establishment of
Weibull constants would have limited application.

The liquid N_2 tests were interesting in that higher strengths were
recorded, yet at least two specimens had fracture origins at particulates.
Charles and Shaw[14] reasoned that in an ambient atmosphere non-critical
cracks grew under the influence of stress corrosion to the critical size
for propagation. Higher strengths were recorded at -196°C because crack
growth cannot occur by this mechanism and higher stresses are required
to propagate a smaller flaw. It would seem that many of the flaws seen in
the ambient tests were <u>not</u> large enough to propagate without added growth
by stress corrosion. Consider the black particulate inclusions in billet 1118
for example. Under ambient conditions, 64.4 kpsi are required for crack
propagation, but at -196°C an average of 91.5 kpsi are required. These
facts suggest several possibilities: (1) the particulate flaws of 40 μm
(Figure 20) may not be large enough and stress corrosion may be required to
extend a surface crack to the flaw with a net crack length that satisfies
the Griffith criterion, or (2) a change in the crack nucleation mechanism
occurs between 23°C and -196°C. The latter possibility might entail a
dislocation nucleated fracture at the higher temperature and a truly brittle
extension of the flaw at -196°C. This would imply that dislocations interact
preferentially with flaws since flaw origins were found at 23°C. Although
possible, this does not appear likely as dislocation mobilities are likely
to be restricted by the imperfect structure surrounding a flaw. Assuming
that the Griffith relation applies and that double cantilever
beam fracture surface energies are applicable, some idea of the necessary
flaw size for fracture can be calculated. Consideration of the recent
measurement of γ for Al_2O_3[21-24] led to the conclusion that the γ = 24.3
J/m^2 value of Swanson[21] was a reasonable compromise value for this calcula-
tion. This calculation gives for the samples in question

at 23°C, 64.3 kpsi - C = 32.2 μm,

Maximum flaw diameter = 64.4 μm,

at -196°C, 91.5 kpsi - C = 16.0 μm

and

Maximum flaw diameter = 32 μm.

Thus, in view of the measured flaw diameter of 40 μm for the black
particulates of Figure 20, further growth by stress corrosion, for example,

might be required to cause fracture at 64.3 kpsi. Based on this fracture mechanics view, model (1) above appears quite reasonable.

G. Conclusions

1. Three commonly used hot pressing grade 99.97% Al_2O_3 powders contain particulate impurities which lead to inclusions and/ or flaws in the product.

2. Four types of defects were found in hot pressed billets where the most severe in terms of limiting strength were particulate inclusions followed by large grains, fine grain patches, and spherical shade zones.

3. Seventy-two percent of the fractures could be traced to a defect in the material. The flaws could not be found in 20% of the specimens, while the remaining 8% could be ascribed to a machining error.

4. Since strengths were shown to be controlled by flaws larger than the grain size, any effort to relate strength to "average" microstructure or method of processing was ruled invalid.

5. A Petch plot can have a non-zero intercept due to the increasing crack/grain size ratio with decreasing grain size. Thus, although microplastic effects are acknowledged as being important in some systems, a non-zero intercept should not, without examination of fracture origins, be considered proof of plastic or anisotropy related fracture initiation.

6. A fracture mechanics view of the strength differences at 23°C and -196°C and particulate flaws at fracture origins led to the conclusion that further crack extension by stress corrosion can be required to cause flaws to be critical.

7. Using a well aligned roller bearing bend fixture, thickness variations in rectangular beam specimens must be under 0.0005 inch to prevent strength limiting stress concentrations.

IV. VOLATILE SPECIES IN HOT PRESSED Al_2O_3

A. General

Upon heat treatment, hot pressed materials normally lose weight and density. This is thought to be a result of processes in addition to pore coalescence which causes "over-firing" in pressureless sintering. The additional mechanisms have been attributed to either the expansion due to an absence of an overpressure of insoluble gases trapped in pores, or the development of gases due to decomposition or reaction of a chemical species in the annealing environment. Rice[25] believes that molecules such as OH^-, SO_4^{-2}, CO_3^{-2} are residual from the powder calcining and subsequent handling

operations. These become entrapped at grain boundaries and pores during
hot pressing. The phenomena persists for vacuum pressed MgO even using
porous or dense dies, and C, Al_2O_3, or Mo die materials. This by itself
implies that the powder is the source of the volatiles. Rossi and Fulrath[26]
in their study of final stage pressure sintering densification of Al_2O_3
found that end point densities can result from gases trapped within the
die during pressing. By alcohol washing the powder, they were able to
reach high density and observe first order kinetics, a fact they attributed
to absorbed H_2O on the surface of the Al_2O_3 crystallites. It appears to
the authors that the possibility of environmental gas entrapment could
also contribute to the problem. The work of Coble[27] on sintering Al_2O_3
demonstrates that the gaseous species present in the furnace influences
the final sintered density. This was interpreted as being a result of
differing gas solubilities where certain gases such as N_2 are sufficiently
insoluble to inhibit the final stage of pore removal. Similar effects
could be operative in pressure sintering. Consequently, there are at least
three possible sources of gases in hot pressed material; decomposition
products from the base salt, volatiles absorbed on powder surface sites, and
entrapment of gases present in the die cavity.

These gases influence properties which, of course, is the main
reason for concern and serious study. The optical properties of transparent
polycrystalline inorganic compounds are seriously downgraded by pore coarsen-
ing. This can be a problem in manufacture and high temperature applications.
It can also be a problem in fabrication as demonstrated by Huffadine et al[28]
for MgF_2 and ZnS. They found it necessary to maintain pressure during the
initial part of the cooling cycle to prevent pore coarsening and an attend-
ent loss of transmissivity. Mechanical properties are also affected by
these phenomena. A slow anneal of MgO can increase ambient temperature
strength presumably due to slow diffusion and volatilization of grain bound-
ary impurities. In contrast, rapid heating to the 1100° - $1300^{\circ}C$ annealing
temperature generates measurable porosity and lowers the ambient strength.
The effect of heating rate and presence or absence of pore generation on
elevated temperature mechanical properties have not been documented in a
controlled fashion. However, density and color changes have been noted during
the course of creep studies on hot pressed Al_2O_3. Many oxides exhibit
strength α (grain size)$^{-\frac{1}{2}}$ relations which break down at grain sizes under
2 μm. In fact, strength has actually been shown to decrease at grain sizes
under 1 μm in MgO and Al_2O_3.[29] One explanation for the phenomena is that
high anion impurities associated with the fine powders and lack of grain
growth lead to decreased grain to grain bond strength.

The ultimate objective of this study is to obtain an understanding
of gas/pore/property relationships in hot pressed Al_2O_3. The initial effort
has dealt with one aspect of this problem: the relationship between powder
precursor, hot pressing environment, and chemistry of volatile species.

B. Experimental

The materials for analysis were selected to test a number of variables.
These samples listed in Table IX consist of both ambient and vacuum hot
pressed Al_2O_3 from the ammonium aluminum sulfate precursor. Also, a sintered
sample from the same precursor was analyzed. Three different powder precursors
were tested for vacuum pressed products, and finally an annealed and

TABLE IX

Alumina Materials for Knudsen Cell Mass Spectrometric Analyses

Sample No.	Powder Vendor	Powder Derivative	Powder Phases Present	Pressing Environment	Sample Condition	Density
459	Ugine 0.2 v/o MgO added	$NH_4Al(SO_4)_2 \cdot 12\ H_2O$	α major γ minor	Ambient	As-pressed	3.986
1368-3	Johnson Matthey	$Al(NO_3)_3$	58 v/o α Al_2O_3 42 v/o γ Al_2O_3	2×10^{-2} mm Hg	As-pressed	3.985
1368-1	Johnson Matthey	$Al(NO_3)_3$	58 v/o α Al_2O_3 42 v/o γ Al_2O_3	2×10^{-2} mm Hg	Annealed	3.985
1245	Linde Laser	$NH_4Al(SO_4)_2 \cdot 12\ H_2O$	γ Al_2O_3 major η, δ Al_2O_3 minor	7×10^{-3} mm Hg	As-pressed	3.980
1650	W.R. Grace 0.1 v/o MgO added	$Al_2O_3 \cdot 3H_2O$	-	8×10^{-2} mm Hg	As-pressed	3.990
Lux-1*	Linde A	$NH_4Al(SO_4)_2 \cdot 12\ H_2O$	α major γ minor	Sintered in H_2	As-received	3.968

*Lucalox from General Electric Co., processing details assumed from various publications.

as-pressed sample were analyzed for one high purity vacuum hot pressed sample from the aluminum nitrate precursor. The latter samples were also chemically analyzed by several techniques.

The mass spectrographic system consisted of an induction heated tungsten effusion cell coupled to a Bendix time-of-flight mass spectrometer. The effusion cell was placed in the vacuum chamber in such a way that gases effusing from the cell passed into the spectrometer ion source by a direct line-of-sight path. This system had the advantage over other possible gas handling systems that unstable species such as free radicals or condensible species could be detected. A movable shutter which could block the line-of-sight path from the cell to the ion source was useful in identifying non-condensible versus condensible gases. It was found during the course of the work that a memory effect required a high temperature degassing of the effusion cell prior to introducing each new sample.

C. Results

Figure 25 illustrates the mass spectrum observed during a typical run, with a background spectrum shown for comparison. The background spectrum is composed of peaks identified with compounds common to most high vacuum systems: H_2O, N_2, and CO, O_2, CH_4, and other hydrocarbons. The spectra taken during the run are characterized principally by a large increase in the contribution from carbon monoxide, CO. This is observed as a large increase in intensity of the mass 28 peak (CO^+). Nitrogen (N_2^+) also exhibits its major mass peak at 28, but CO and N_2 can be distinguished easily by comparison of their complete mass spectra. Under electron impact, molecular nitrogen undergoes ionization and dissociation to produce the ions N_2^+ (mass 28), N^+ (mass 14), and N_2^{++} (mass 14), while carbon monoxide yields ions CO^+ (mass 28), O^+ (mass 16), CO^{++} (mass 14) and C^+ (mass 12). The spectrum shown in Figure 25 shows large increases in intensity of peaks at masses 12 and 16 as well as at mass 28, but only a slight increase at mass 14, identifying the evolved gas as carbon monoxide.

Above $1300^\circ C$ the mass spectrum for Sample 459 showed peaks at masses 70 and 27 as illustrated in Figure 25. The movable shutter identified these gases as condensible, indicating the presence of Al_2O and Al, respectively. These species have been previously seen by DeMaria et al[30] when Al_2O_3 is heated in a reducing atmosphere. The major difference between the present study and that referenced is that evolution of Al_2O and Al began at a much lower temperature for the present work, indicating the presence of stronger reducing conditions.

A chip of Lucalox was heated to a maximum temperature of $1670^\circ C$ without any identifiable Al_2O or Al peaks. Some CO evolution occurred, but much less than for Sample 459. This experiment was repeated twice with similar results*. The lack of Al_2O or Al for Lucalox suggests that C is present in hot pressed billet 459, resulting in the reaction:

$$2 \; Al_2O_3 \; (s) + 5 \; C \; (s) \longrightarrow Al_2O \; (g) + 2 \; Al \; (g) + 5 \; CO \; (g) \quad (1)$$

---
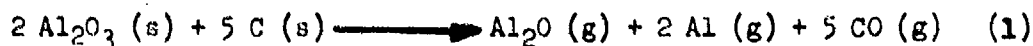
*McRae[31] also observed CO (mass 28) evolved from Lucalox and attributed it to dissolved, chemisorbed and occluded gases.

(a)

70
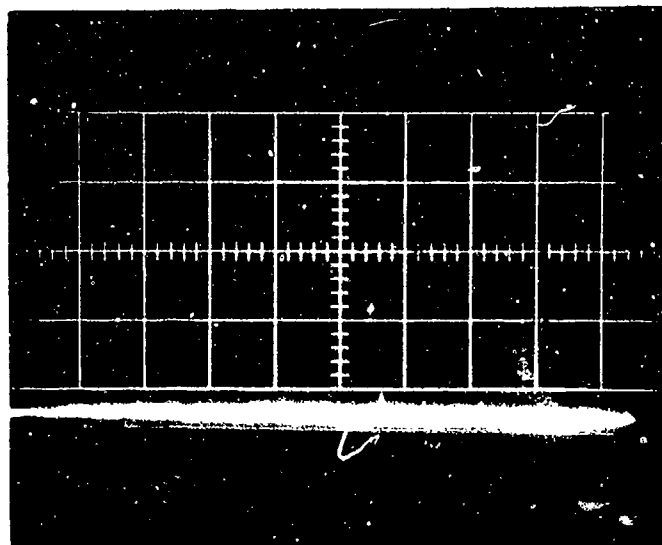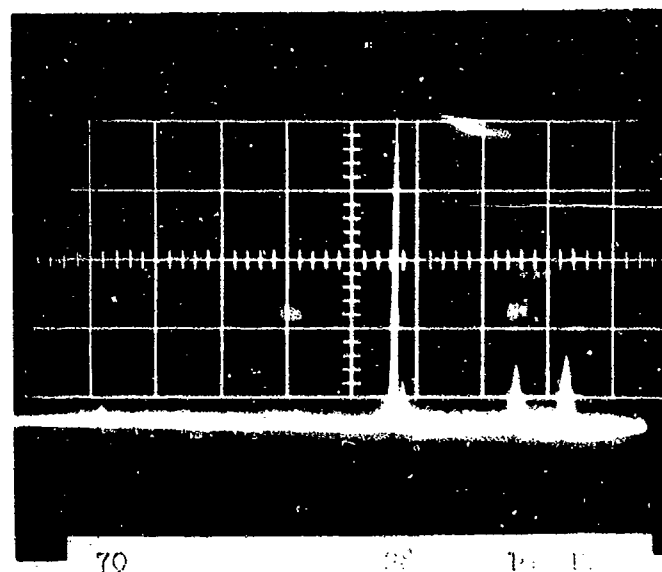
(b)

Figure 25.   Mass spectrum (a) background, and (b) sample 459 at 1500°C
showing evolved Al₂O (mass 70), CO⁺ (mass 28), and Al (mass 27).

Many of the hot pressed samples listed in Table IX did not exhibit the presence of Al_2O and Al in heating to $1550^\circ C$. Thus, reaction (1) does not appear to be dominant in all grades of hot pressed materials.

The samples listed in Table IX were traversed to $1550^\circ C$. Sample 459 was heated twice. The dominant species that was clearly identified as being evolved from the Al_2O_3 samples was mass 28. The portion above background was judged to be CO as discussed previously. Because Al_2O and Al were not observed on all samples, it appears likely that CO gas rather than C is entrapped for many grades of hot pressed Al_2O_3. This particular question was not fully resolved at this point in the study, and will be discussed further. Sample 1245, a sulfate derived Al_2O_3, was taken through its melting point without any sign of a S related species. Upon melting, there was a massive evolution of CO which swamped the electronics.

The relative intensity of mass 28 was recorded versus time at each of 4 temperatures from $930^\circ C$ to $1550^\circ C$. Quantitative data was not recorded for the initial heating of sample 459, however. As each new temperature was reached, the mass 28 peak height rose through a maximum and decayed to a nearly constant value. These values are proportional to concentration, but, of course, are arbitrary units.

It was reasoned that the concentration evolved would be proportional to the surface area of the sample. Thus, the peak heights were divided by surface area and plotted versus reciprocal temperature in Figures 26 and 27 for the maximum concentration and near steady state value, respectively. The near steady state concentration values (Figure 27) for Samples 1245, 1650, and Lux-2 appear to rise with temperature as expected for a thermally activated process. The peak concentrations also show this trend at all but the lowest temperature where high concentrations of CO were evolved. This low temperature phenomena is undoubtedly a result of initial degassing of the surface. As the temperature was increased, CO apparently diffuses from the interior of the specimen and is desorbed. Such a process probably involves an activation energy of motion explaining the higher concentrations at high temperatures. In contrast, Samples 1368-1 and 1368-3 exhibited approximately equal concentrations of CO evolution at all temperatures. This can be explained as resulting from desorption of the surface or a near surface layer. The downward trend of concentration with increasing temperature suggests a slow depletion of this surface layer. The initial heating of the ambient hot pressed sample 459 gave qualitative evidence for massive CO evolution (Figure 25). However, the second heating of the same sample (Figures 26 and 27) demonstrated that the CO evolution was rather low. This is taken as further evidence for a slow depletion of a surface layer.

Chemical analyses have been performed on powder, pressed, and annealed samples from Johnson Matthey Al_2O_3. Samples 1368-3 and 1368-1, analyzed in these experiments, are representative of the latter two types of samples. Table X lists these analyses of possible volatile species performed by a variety of techniques. A factor of 4 disagreement among the techniques is noted. Greater confidence is placed in the wet chemical, fusion and spark source mass spectrometry analyses than the plasma source mass spectrometry. It is interesting to note that according to the fusion analysis, C actually decreased as a result of hot pressing. Since the
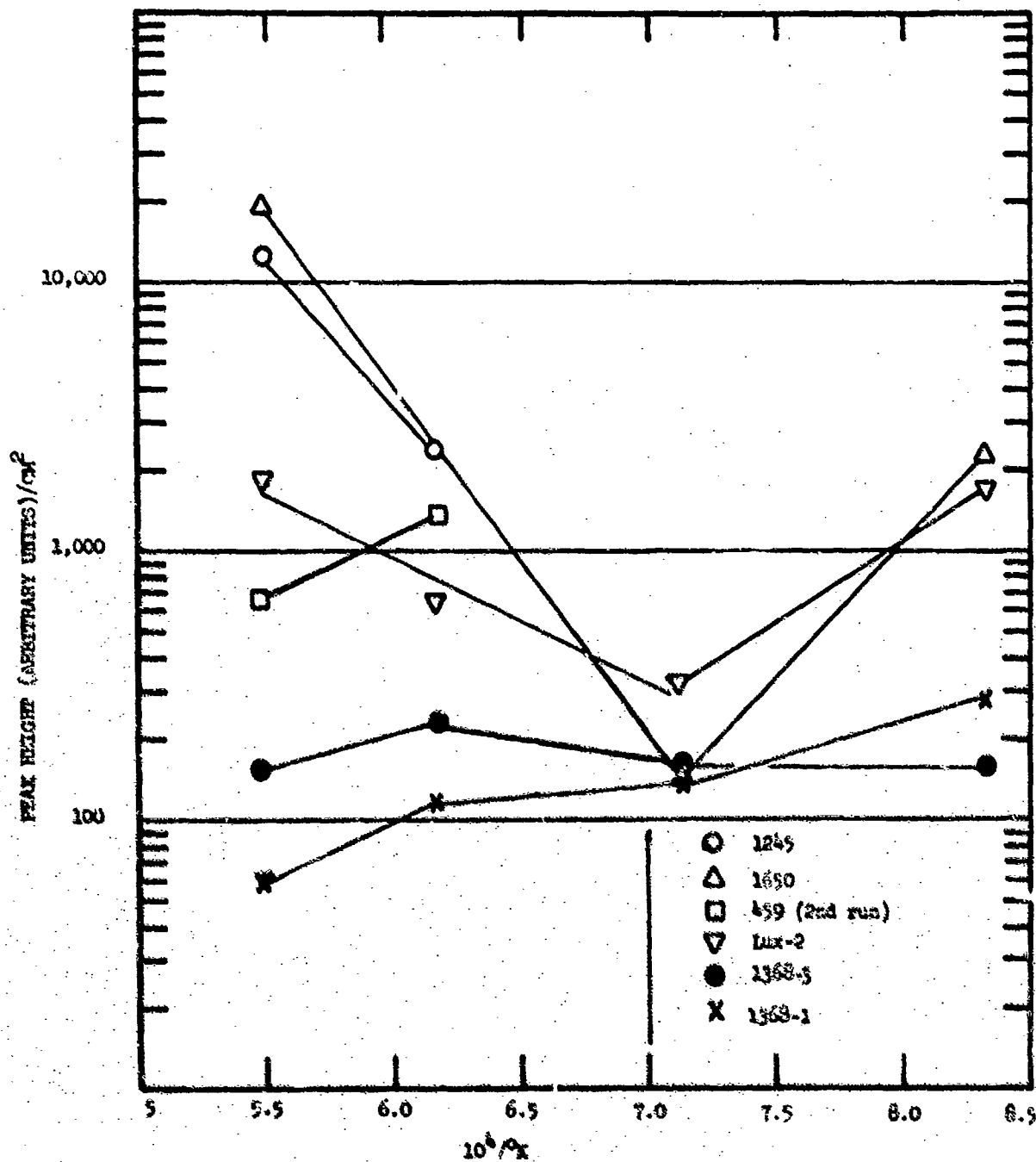
Figure 24. Peak Specific CO Evolution Versus Temperature for Various Grades of Hot Pressed and Sintered Al_2O_3.
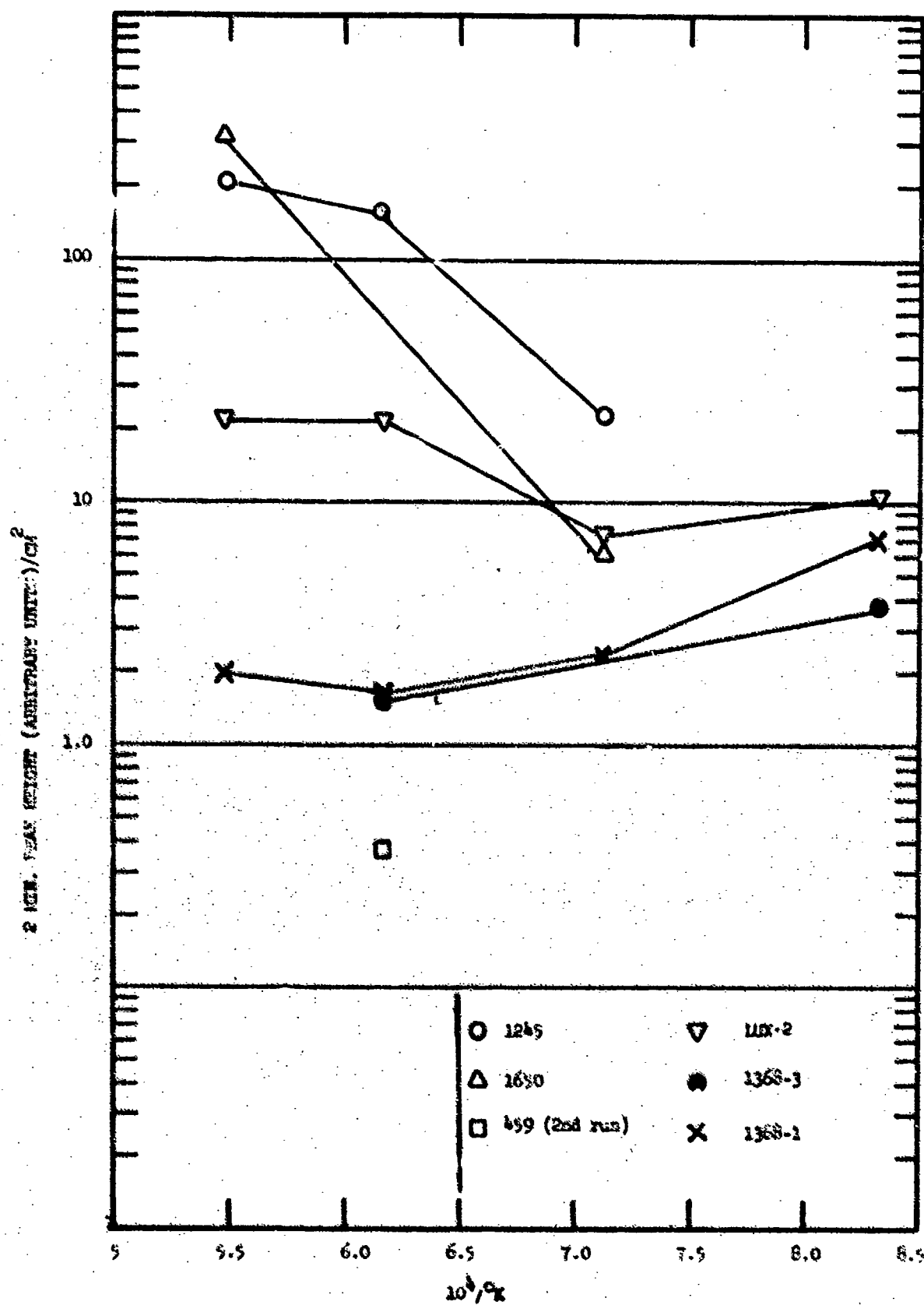
Figure 27. Apparent Steady-State Specific CO_2 Evolution Versus Temperature for Various Grades of Hot-Pressed and Sintered Al_2O_3.

Legend:

○	1245	▽	118X-2
△	1630	●	1368-3
□	499 (2nd run)	✕	1368-1

y-axis: 2 KM. PEAK HEIGHT (ARBITRARY UNITS)/cm^2

x-axis: $10^4/°K$

TABLE X

Anion Analysis of Impurities in High Purity Alumina*

Element	Technique	Concentration in ppmw for Samples		
		Powder	As-Pressed	Annealed
C	Plasma mass spec.	5	18	-
	Fusion	800	80	
F	Plasma mass spec.	420		
	Spark mass spec.	4	4	10
	Wet chemical		18	
Cl	Plasma mass spec.	<0.3		
	Spark mass spec.	50	40	15
S	Spark mass spec.	10	10	10

Analysis of material equivalent to 1368-1 and 1368-3.

sample was prepared into a powder for analysis, some CO entrapped during
pressing could probably be lost to the atmosphere at this point. The plasma
source mass spectrometric analysis shows a gain in C during pressing. This
analysis was performed on a solid sample, thus it might include entrapped
CO. Based on the analyses alone, Cl is the only other species that can be
expected to be evolved during the Knudsen cell heating, and none was seen.

The weight loss during the Knudsen cell experiments is listed in
Table XI. For the hot pressed samples the weight losses correlated
qualitatively with the amount of CO evolved at the maximum temperature;
the correlation is better for the weight loss normalized per unit area of
the sample than per unit mass as would be expected if the loss of CO were
diffusion limited. This did not hold for the sintered sample, Lux-2, which
did not lose weight, but apparently evolved CO. Hot pressed sample 459
was large enough to make accurate density measurements before and after its
two Knudsen cell heating runs. The initial density gain was quite unexpected
as it was felt bloating would occur due to the rapid heating; a small density
loss was recorded for the second heating. The change in density is thought
to be real, as density was measured four times with standard deviations of
$\pm$ 0.007 gm/cc and $\pm$ 0.004 gm/cc.

These total weight losses are very much higher than can be accounted
for by carbon present simply from gas entrapped in the pores at the point
of pore closure. Assuming that the pores contain CO at 1 atm. pressure
and that closure occurs at 7% porosity, the entrapped carbon would be only
2 ppm, and for vacuum hot pressed material the carbon content from entrapped
gas would be even lower. This is orders of magnitude less than the 80 ppm
measured for the high purity, vacuum hot pressed material, or than carbon
contents as high as 470 ppm[32] measured on other hot pressed Al_2O_3. Much
of the observed weight loss can be accounted for on the basis of these
higher carbon contents assuming some reduction and vaporization of Al_2O_3
as in equation 1. These results both indicate that there is significantly
more carbon present than that entrapped as gas at pore closure. Since
these powders are not carbonate derived and the carbon contents are higher
than usually measured for the powder, it seems probable the carbon is picked
up from the hot pressing dies. It is difficult to know the driving force
for transport or the form of the carbon in Al_2O_3 since there are no solubil-
ity data for C, CO, or CO_2 in Al_2O_3. Both solid diffusion and gas transport
could provide mass transport from the die to increase the C and CO to the
solubility limits. Carbon could also be present as a second phase. Because
of the temperature dependence of the equilibrium CO/CO_2 ratio this could
result from gaseous transport and redeposition of solid carbon in the compact
during heating when the temperature of the die is greater than that of the
compact. Physical inclusion during loading could also be a contributor
although care is taken to eliminate this. A final possibility is reduction
of Al_2O_3 to form Al_4C_3 or oxycarbides; however, the thermodynamics do not
appear to favor this under the hot pressing conditions before pore closure,
and there is little microstructural evidence for it.

In spite of the uncertainty as to the form of most of the carbon
present, it is of interest to consider briefly the form of the gas which
is entrapped at pore closure. After closure, the pore can shrink to an
equilibrium size at which the internal pressure is in equilibrium which

TABLE XI

Correlation of Physical Change with Gas Evolution

in Knudsen Cell Heating Experiments

Sample	ΔW, %	$\frac{\Delta W}{gm/cm^2} \times 10^4$	$\Delta \rho$, %	1550°C CO Peak Height
1245	-0.63	7.6		12,650
1650	-0.55	8.9		19,000
459 1st	-0.37	11.5	+0.175	(high qual. only)
2nd	-0.035	1.0	-0.091	69
1368-3	-0.083	1.1		153
1368-1	-0.040	0.6		59
Lux-2	0	0		1825

the externally applied pressure and the surface tension, assuming spherical pores:

$$p_i = \frac{\partial \gamma}{r} + Pa$$

where r is the pore radius, p_i the internal pressure, Pa the external pressure, and γ the surface energy. Assuming the gas to be present at the ambient pressure at closure (which in hot pressing is less than the applied pressure) and assuming ideal gas behavior the equilibrium pore size and final density can be easily calculated. This has been done neglecting gas solubility, taking the porosity at closure as 7% and using 1000 erg/cm^2 for γ and is plotted in Figures 28 and 29 as a function of the initial pore size at closure. These were calculated for ambient hot pressing taking $p_o = 1$ atm. and for vacuum pressing using $p_o = 10^{-3}$ atm., which is higher than the measured vacuum levels to account for the low powder permeability. The calculations are done for an applied pressure of 5000 psi and for ambient pressures which would be typical of sintering and also of the conditions for equilibration in firing hot pressed bodies at ambient pressure. For these materials with 1-2 μ grain size, it is expected that most of the pores would be between 0.1 and 1 μ at closure. It is interesting that for such fine grain sizes the final porosities are less than 0.1% even for ambient pressing and further the amount of bloating on refiring is small to insignificant. For vacuum pressing the equilibrium porosity and bloating on refiring for small pores are too small to be measurable. This indicates that bloating must result from larger pores present at closure or from gaseous diffusion between pores during hot pressing and during refiring. For the fine pore size predicted, the internal pressures are very high and gas solubility may be expected. Coble[33] has treated this analytically, showing that for fine pores, solubility becomes increasingly important, but there are no CO or CO_2 solubility data to allow quantitative analysis. These considerations plus frequent observation of bloating on refiring, suggest that the solubility and diffusivity of the CO is sufficient to allow some pore coarsening during hot pressing or refiring of this fine grained Al_2O_3.

The view that emerges is that two simultaneous phenomena are contributing to the weight loss and CO evolution: (1) C is reacting with Al_2O_3 according to equation (1); and (2) CO gas is entrapped and diffuses along grain boundaries to the surface and desorbs. There does appear to be a correlation of gas evolution with powder precursor. The sulfate and trihydrate derived powders are associated with high evolution, whereas the nitrate gave a low evolution. Some CO was present in the as-pressed material, however, as the annealed sample (1368-1) evolved lower concentrations. The study to date has not adequately defined the differences between vacuum and ambient hot pressed Al_2O_3. Clearly they both evolve high concentrations of CO, and further work is required on this latter point.

Annealing and the effect of annealing on pore composition and pore volume has received only introductory attention, and the results were quite surprising. It can definitely be concluded that ambient hot pressed Al_2O_3 can, under some conditions, be rapidly heated, evolving copious quantities of CO with an apparent improvement to the pore structure reflected by an increased bulk density. The limits of this condition will be the subject of further studies.
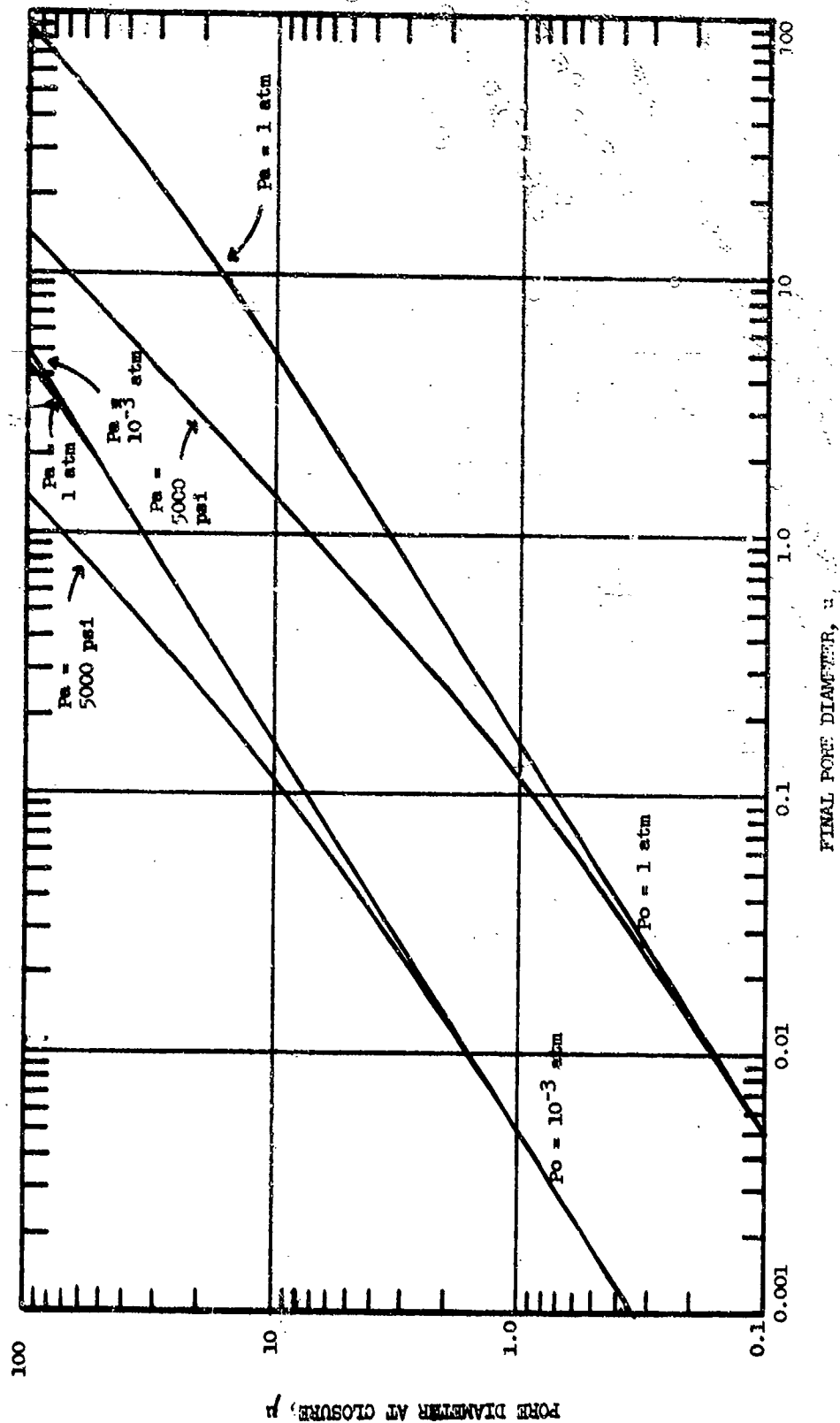
Figure 28. Equilibrium Pore Size as a Function of Initial Pore Size at Closure and Applied Pressure for Ambient and Vacuum Hot Pressing Assuming No Gas Solubility.
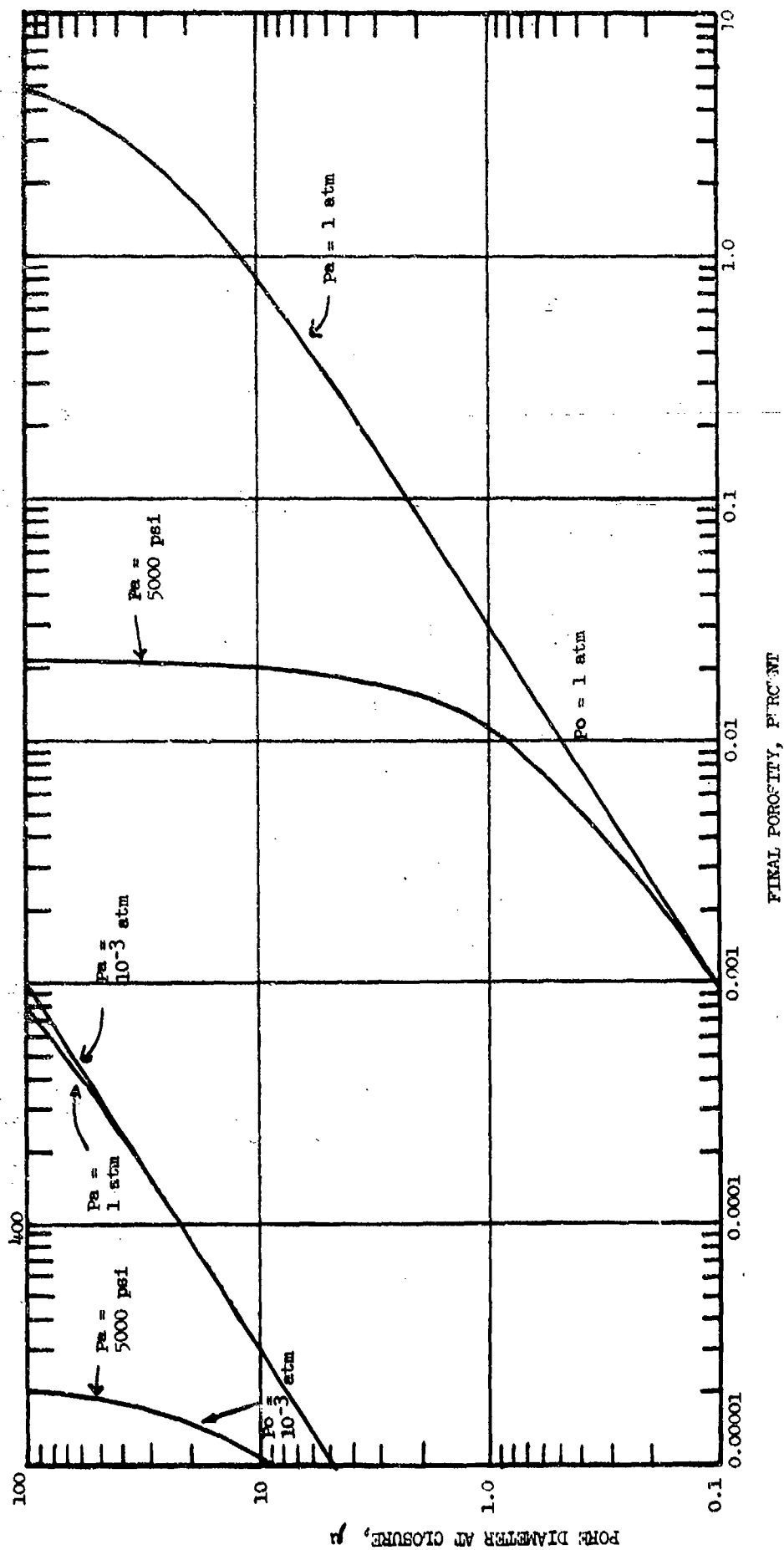
FINAL POROSITY, PERCENT

PORE DIAMETER AT CLOSURE, μ

Figure 29. Limiting Porosity from Insoluble Gases as a Function of Initial Pore Size and Applied Pressure.

The findings to date are somewhat in contrast to those of Rice[21] who reported CO, OH, H_2O, CO_2, and mass 34 (H_2S) to be evolved from hot pressed Linde A Al_2O_3. The current effort found no evidence for mass 34. This is especially surprising since sample 1245 was fabricated from a γ Al_2O_3 derived from $NH_4Al(SO_4)_2 \cdot 12 H_2O$ which, of course, means that it received less calcination than the powder used by Rice which, if it was standard Linde A, contained α Al_2O_3 as a major phase and only minor γ Al_2O_3. Also, although OH, H_2O and CO_2 were observed, it was judged that these could be assigned to a background source.

D. Conclusions

1. The major species evolved from Al_2O_3 hot pressed in graphite dies is CO which is thought to be entrapped from the pressing environment. The evolution results in a weight loss which is proportional to the CO evolved.

2. There appears to be a correlation between the CO evolved and the Al_2O_3 precursor. The $Al(NO_3)_3$ derived powder evolved markedly lower concentrations of CO.

3. The evolution of CO seems to be limited by a kinetic process. The nature or mechanism of the process has not been analyzed.

4. No gaseous species directly related to the powder precursor was observed during Knudsen cell heating to $2000°C$ for a sulfate derived powder or to $1550°C$ for the other powders.

5. Although a loss of density has been observed upon rapid heating of hot pressed Al_2O_3, similar heating conditions can result in an increased density and massive evolution of CO.

V. PRESS FORGING Si_3N_4

A. General

Silicon nitride has become an important engineering material. Many laboratories are engaged in efforts to improve the properties and fabricate shapes. Hot pressing experiments conducted at Avco[34] and Westinghouse[35] suggested that a slight preferred orientation is developed during a conventional hot pressing cycle. This suggested that a press forging approach similar to that employed for Al_2O_3 might provide the ability to achieve unique shapes and/or properties. Several preliminary experiments are reported in this section.

B. Materials

High α Si_3N_4 powder* was ball milled with 4% MgO using an Al_2O_3 ball mill and alcohol media. (Subsequent work has shown that WC balls and tertiary butanol provide a superior mixing procedure.)[35] The dried powder was cold pressed into a 2-inch diameter by 1-inch high preform for a flat disc forging and a 1-inch diameter by 1-inch high preform for a hemispherical forging.

---

*Advanced Materials Engineering Ltd.

C. Results and Discussion

The forging conditions and results are listed in Table XII. The 95% of theoretical density for 1771 was considered reasonable for the first attempt, but certainly not outstanding. The billet was flat, with only minor edge cracking, indicating an extensive capacity for forging.

The hemispherical forging, 1788, was quite successful. Rim cracks were restricted to the disposable skirt. A sound moderately high density full hemisphere was obtained as shown in Figure 30. The hemispherical surface illustrated is an "as-pressed" surface. The forging die fractured on this run pointing to one problem that must be considered in future work. It is thought that thermal expansion mismatch between the die and product produced the strain to fracture in the cool down cycle. A hot extraction procedure must be devised.

A strong microstructural texture was observed in sample 1771 (Figure 31). This is an extremely strong microstructural texture and compares with any of the press forged Al_2O_3 samples examined.[1]

The sample was analyzed by X-ray analysis with the phase analysis reported in Table XIII. This billet was higher in retained Si_2N_2O than had been seen on a recently completed program.[34] This is probably due to the fact that the sample was unconfined and porous up to $1700^\circ C$, the temperature of forging. The retention of a minor amount of α-Si_2N_4 is common as is the finding of a trace concentration of Fe_3Si which is an impurity coming from the starting Si in the powder production.

TABLE XIII

Phase Analysis of Press Forged Si_3N_4 (1771)

| Phase	Concentration Percent
β-Si_3N_4	72
α-Si_3N_4	2
Si_2N_2O	26
Fe_3Si (tentative)	trace

An inverse pole figure for β-Si_3N_4 phase was prepared from an area on a polished surface normal to the pressing direction located approximately 0.5 inch from the rim. The analytical technique was identical to that described in Section II. Some possible interference was expected from the α-Si_3N_4, but because of the low concentration the interference was predicted to be small. The pole figure is shown in Figure 32. Also indicated on this plot are maximum possible errors due to instrumental variation. The plot shows a moderate crystallographic orientation with the "c" axis normal to the pressing direction. The Si_2N_2O phase, which is orthorhombic, exhibited a lesser degree of orientation with the "b" axis normal to the pressing direction. This orientation is compatible with the

TABLE XII

Si₃N₄ Press Forging Conditions and Results

Experiment	Temp. °C	Pressure Kpsi	Time	Density gm/cc	Remarks
1771	1700	6000	75	3.03	0.2" rim cracks
1788	1750	3500	20	3.09	Sound, several rim cracks confined to skirt.
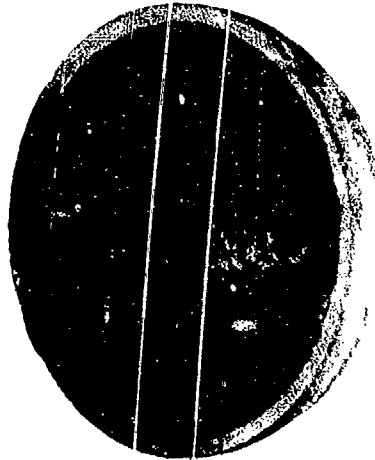
#5766-1
1X

Figure 30. Si_3N_4 Hemisphere Forged from a Cold Pressed Preform

72449   7500X

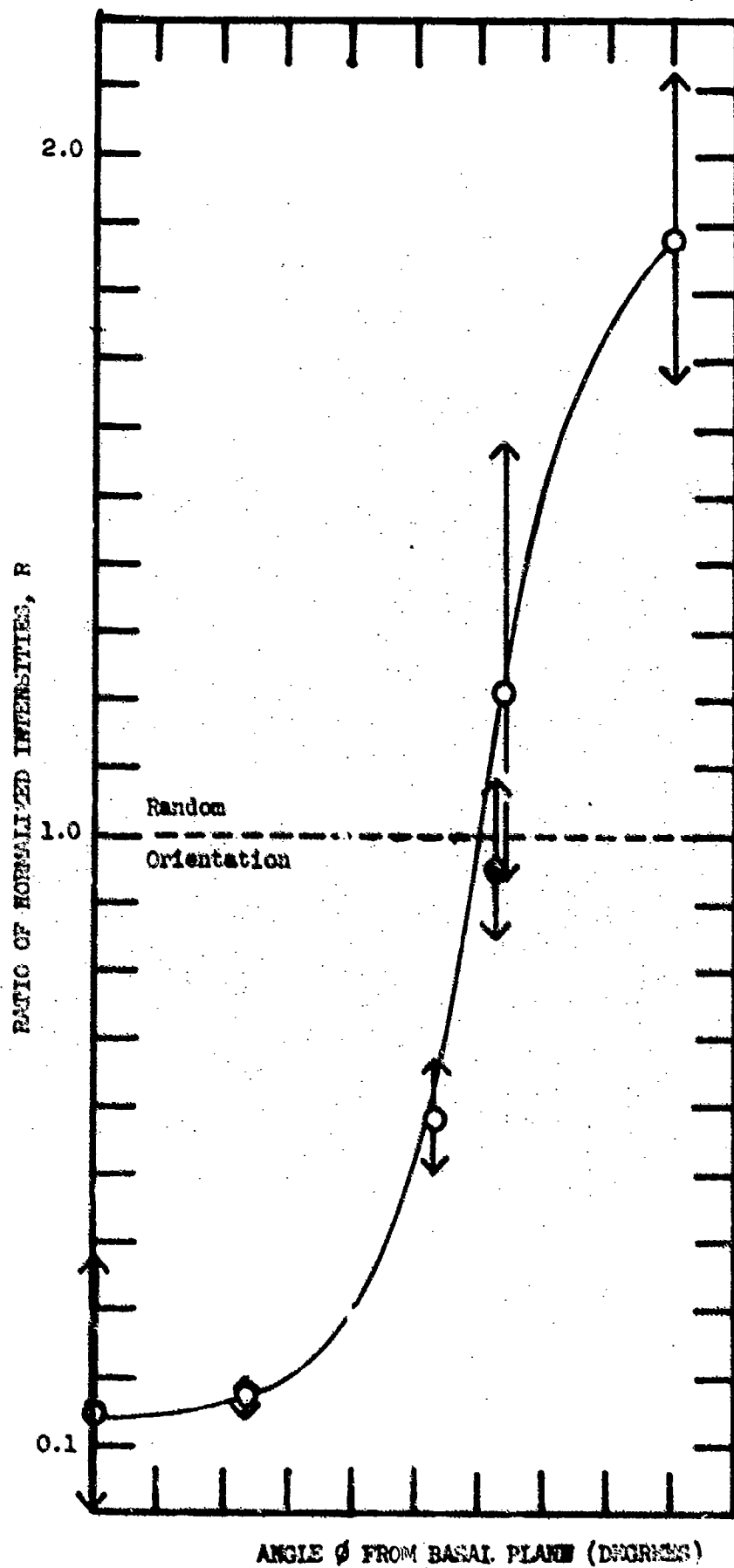Figure 31. Microstructural Texture in Press Forged Si_3N_4, Sample 1771.

Figure 32. Inverse Pole Figure for Press Forged Si₃N₄

$\{10.0\}<00.1>$ slip system where the slip pla⌐ rotates normal to the applied force due to shear within grains oriented favorably for slip.

Four point bend strengths and unnotched Charpy mode impact strengths were measured on billet 1771. These are reported and compared with two hot pressed Si_3N_4 billets prepared on another program[34] in Table XIV. Hot pressed billet 1810 was fabricated with powder prepared in a similar manner to that employed for this forging. Hot pressed billet 1851 contained 1% MgO and was the powder prepared by a special milling technique. This milling technique has been shown to give higher fracture surface energies and higher strengths for reasons that are not understood.[35] Similar results are noted in Table XIV, thus a comparison of billet 1771 with 1851 is not totally valid. It is interesting to note the higher impact strength and lower bend strength at $1316^{\circ}C$. A comparison of the properties of 1771 with 1810 again shows that the $1316^{\circ}C$ impact strength was somewhat higher for the forged billet. Both the $23^{\circ}C$ and $1316^{\circ}C$ strengths were lower for the forged billet; however, the $1093^{\circ}C$ strength may be judged to be equivalent to either billet 1810 or 1851. Attention is called to the fact that forged billet 1771 was only 95% dense whereas the other two were 99% dense. In summary, it appears that forging holds promise in terms of matching the low temperature properties of hot pressed Si_3N_4. At $1316^{\circ}C$ a low bend strength, together with a high impact strength, suggests that the microstructure texture results in increased plasticity. Clearly, further work to delineate the nature and usefulness of the high temperature behavior is warranted.

D. Conclusions

1. Si_3N_4 can be press forged into sound dense discs or hemispherical shapes, thus the process appears to hold promise for application to this material.

2. A strong microstructural and moderately strong $\{10.0\}$ texture is developed.

3. Press forged Si_3N_4 exhibits an interesting interrelationship between high temperature bend and impact strength which warrants further work.

TABLE XIV

Comparative Strength of Si₃N₄ Billets

Specimen	Bend Strength in Kpsi			Impact Strength on ¼ x ¼ Inch Section, in.-lb.		
	23°C	1093°C	1316°C	23°C	1093°C	1316°C
1771 - Forged 1% MgO - Regular Milling - 3.03 gm/cc	80.8 86.5 79.5	69.0 63.3 43.4	26.9 28.0 23.6	1.63		4.83
Av.	82.3	59.6	26.2			
1810 - Hot Pressed 1% MgO - Regular Milling - 3.15 gm/cc	102.2 89.7 80.3	69.5 58.5 63.3	39.2 38.5 38.6	2.24	4.50	3.14
Av.	90.7	63.8	38.8			
1851 - Hot Pressed 1% MgO - Special Milling - 3.18 gm/cc	134.9 119.3 116.4	62.7 65.9 52.1	37.5 46.2 41.1	3.95	2.63	3.50
Av.	123.5	62.7	41.0			

VI. REFERENCES

1. a) W.H. Rhodes, D.J. Sellers, A.H. Heuer, and T. Vasilos, "Development and Evaluation of Transparent Aluminum Oxide," N1/6-8986, Final Report (June 1967).

   b) A.H. Heuer, D.J. Sellers, and W.H. Rhodes, J. Am. Ceram. Soc., 9, 468 (1969).

   c) A.H. Heuer, W.H. Rhodes, D.J. Sellers and T. Vasilos, "Microstructure Studies of Polycrystalline Refractory Oxides," NOw-66-0506(d), Summary Report (1967).

   d) W.H. Rhodes, D.J. Sellers, R.M. Cannon, A.H. Heuer, W.R. Mitchell, and P.L. Burnett, "Microstructure Studies of Polycrystalline Refractory Oxides," Contract N00019-67-C-0336, Summary (1968).

   e) W.H. Rhodes, P.F. Jahn, P.L. Burnett, "Microstructure Studies of Refractory Polycrystalline Oxides," Contract N00019-68-C-0108, (June 1969).

   f) W.H. Rhodes and R.M. Cannon, "Microstructure Studies of Refractory Polycrystalline Oxides," Contract N00019-69-C-0198, (December 1969).

   g) W.H. Rhodes and R.M. Cannon, "Microstructure Studies of Refractory Polycrystalline Oxides," Contract N00019-70-C-0171.

   h) W.H. Rhodes, P.L. Berneburg, and R.M. Cannon, "Microstructure Studies of Refractory Polycrystalline Oxides," Contract N00019-71-C-0325.

2. R.L. Coble, J. Am. Ceram. Soc., 45, 123 (1962).

3. R.M. Cannon and W.H. Rhodes, "Deformation Processes in Forging Ceramics," Summary Report, Contract NASW-2187.

4. A.M. Lejus, Bull. Soc. Chim., pp. 2123 (1962).

5. S.K. Roy and R.L. Coble, J. Am. Ceram. Soc., 51, 1 (1968).

6. D.A. Gryvnak and D.E. Brurch, J. Opt. Sci. Amer. 55, 625 (1965).

7. "Optical Properties and Applications of Linde Cz Sapphire," Technical Bulletin, Union Carbide Corp.

8. N. Grimm, G.E. Scott, and J.D. Sibold, Bull. Am. Ceram. Soc., 50, 962 (1971).

9. I.H. Malitson, F.W. Murphy, Jr., and W.S. Rodney, J. Opt. Soc. Am., 48, 72 (1958).

10. C.D. Pears and H. Starrett, "An Experimental Study of the Weibull Volume Theory," AFML-TR-66-228.

11. D.L. Vrooman and J.E. Ritter, Am. Ceram. Soc. Bull. 49, 789 (1970).

12. E.B. Shad, J. Am. Ceram. Soc., 48, 43 (1965).

13. H.P. Kirchner, R.M. Gruver, ａ .. Walker, J. Am. Ceram. Soc., 56, 17 (1973).

14. R.J. Charles and R.R. Shaw, "Delayed Failure of Polycrystalline and Single Crystal Alumina," General Electric Report No. 62-RL-3081M.

15. B.J. Hockey, Proc. Brit. Ceram. Soc., 20, 95 (1972).

16. R. Rice and P.F. Becher, Am. Ceram. Soc. Bull., 50, 374 (1971).

17. E.M. Passmore, R.M. Spriggs, and T. Vasilos, J. Am. Ceram. Soc., 48, 1 (1965).

18. R.M. Spriggs, J.B. Mitchell, and T. Vasilos, J. Am. Ceram. Soc., 47, 323 (1964).

19. R.W. Rice, Proc. Brit. Ceram. Soc., 20, 205 (1972).

20. a) Carniglia, S.C., J. Am. Ceram. Soc., 48, 580 (1965).
    b) Carniglia, S.C., Am. Ceram. Soc. Bull., 50, 184 (1971).

21. G.D. Swanson, J. Am. Ceram. Soc., 55, 48 (1972).

22. P.L. Gutshall and G.E. Gross, Eng. Fract. Mech. 1, 463 (1969).

23. G.D. Swanson and G.E. Gross, J. Am. Ceram. Soc., 51, 602 (1968).

24. L.A. Simpson, J. Am. Ceram. Soc., 56, 7 (1973).

25. R.W. Rice, Proc. Brit. Ceram. Soc., 12, 99 (1969).

26. R.C. Rossi and R.M. Fulrath, J. Am. Ceram. Soc., 48, 558 (1965).

27. R.L. Coble, J. Am. Ceram. Soc., 45, 123 (1962).

28. J.B. Huffadine, A.J. Whitehead, and M.J. Latimer, Proc. Brit. Ceram. Soc., 12, 201 (1969).

29. R.M. Spriggs, T. Vasilos, and L.A. Brissette, Mat'l. Sci. Res., 3, 313 (1966).

30. G. DeMaria, J. Drowart and M.G. Inghram, J. Chem. Phys., 30, 318 (1959).

31. P.C. McRae, Bull. Am. Ceram. Soc., 48, 559 (1969).

32. D. Sellers and J.E. Niesse, "The Development of Hot Pressed Alumina for Gas Bear: ｇ Applications," Final Report, Contract N00030-66-C-0189 (28 February 1969).

33. R.L. Coble, "Final Stage Sintering: Atmosphere Effects," Phys. of Sintering, 1/3 F1, (1969).

34. W.H. Rhodes, and R.M. Cannon, Jr., "High Temperature Compounds for Turbine Vanes," NASA-CR-120966.

35. F.F. Lange and G.R. Terwilliger, "Fabrication and Properties of Silicon Compounds," Final Report, Contract N000-19-17-C-0107.

36. E. Butler, Phil. Mag., 24, 829 (1971).